# Simulation-based consequence models of seismic direct loss and repair time for archetype reinforced concrete frames

Karim Aljawhari [a,b,*], Roberto Gentile [b], Carmine Galasso [a,b]

[a] *Centre for Training and Research on Reduction of Seismic Risk (ROSE), Scuola Universitaria Superiore (IUSS) Pavia, Pavia, Italy*
[b] *Department of Civil, Environmental & Geomatic Engineering, University College London (UCL), London, United Kingdom*

ARTICLE INFO

ABSTRACT

Seismic risk management of building portfolios requires a reliable evaluation of earthquake-induced losses. This is commonly performed using consequence models linking structure-specific damage states (DSs) experienced by a building to a given loss metric (or decision variable). This study demonstrates a simulation-based procedure that derives refined probabilistic consequence models considering two essential loss metrics: direct-loss and repair-time ratios (repair cost or time normalised by the corresponding reconstruction values). Nine case-study reinforced concrete frames with various heights and design-code levels are developed to represent common residential buildings in Italy and the Mediterranean region. The proposed procedure starts by defining building-level, structure-specific DSs that reflect the increasing structural and nonstructural damage for the nine frames. Their seismic response is then assessed by analysing two-dimensional nonlinear numerical models and deriving building-level fragility relationships. Next, component-based direct-loss and repair-time analysis is conducted via the FEMA P-58 methodology, which computes such metrics at multiple ground-shaking intensities using Monte Carlo sampling. The consequence models are finally characterised by fitting probabilistic distributions to the direct-loss and repair-time realisations after conditioning them on the respective global DSs sustained by each case-study frame. This procedure enables deriving enhanced consequence models that can be easily implemented in risk analysis of building portfolios to obtain quick loss estimates. This study finally sheds some light on the possibility of correlating repair time to direct loss, which might be useful in estimating indirect losses resulting from downtime, particularly in cases where repair-time data or models are unavailable.

## 1. Introduction

Moderate-to-strong earthquakes still result in devastating consequences around the globe, leading to severe economic losses, casualties, and disruption to vital life aspects, as demonstrated by several past events [1]. Seismic losses include direct losses associated with the repair cost of earthquake-damaged structural and nonstructural building components, in addition to indirect ones incurred due to downtime and its resulting business interruption. Downtime, in turn, includes two components: 1) the "rational" component defined as the time required to accomplish repair works (or simply repair time); 2) the "irrational" component, which is the timeframe between the seismic event and the initiation of repair work, covering the duration needed for activities like bidding, financing, and resource mobilisation [2].

To effectively manage/mitigate the above consequences, reliable quantification of seismic performance/losses against potential ground-shaking scenarios is required to identify vulnerable structures requiring intervention. This has led to developing the performance-based earthquake engineering (PBEE) computational framework, providing decision-makers with an improved seismic performance characterisation in terms of meaningful decision variables (DVs) (*e.g.*, repair costs, downtime). The past few decades have witnessed the widespread implementation of PBEE, particularly in its probabilistic framework introduced by the Pacific Earthquake Engineering Research (PEER) center [3]. This framework estimates seismic risk, *i.e.*, the (mean) annual frequency of exceeding a specific DV, by integrating four analysis phases: site-specific hazard analysis, structural response analysis, damage evaluation, and loss estimation, along with their uncertainties. The current state-of-the-art/practice in building-specific risk assessment is the component-based methodology proposed in the Federal Emergency Management Agency (FEMA) P-58 guidelines [4]. This methodology represents a refinement/practical implementation tool of

* Corresponding author. Centre for Training and Research on Reduction of Seismic Risk (ROSE), Scuola Universitaria Superiore (IUSS) Pavia, Pavia, Italy.
*E-mail address:* karim.aljawhari@iusspavia.it (K. Aljawhari).

the PEER framework; it estimates the seismic loss in a building by aggregating the losses incurred by its individual components.

Although the FEMA P-58 is deemed a robust and rigorous methodology, it is arguably more applicable to individual structures than large-scale building portfolios. This is due to its time-intensive nature and complexity, which requires defining a comprehensive inventory of all damageable (vulnerable) structural and nonstructural components in a building. These components must be associated with 1) fragility models defining the probability of exceeding multiple component-specific damage states (DSs) given a measurable engineering demand parameter (EDP); 2) consequence models describing the component-loss distribution for each DS. This information is location-specific and might not always be available. Any missing fragility/consequence models can be developed via laboratory testing of individual components and collecting post-earthquake loss data, but this is presumably beyond resources in large-scale seismic risk applications. Furthermore, the reliability of FEMA P-58 risk assessment depends markedly on the accuracy of the building's nonlinear response simulated via numerical modelling. Hence, using advanced multi-degree-of-freedom (MDoF) nonlinear models is preferable to ensure reliable loss estimates.

The previous tasks become more cumbersome in the case of building portfolios as component inventories must be defined for a large number of "archetype" buildings reflecting specific exposure and vulnerability typologies (or classes). Refined MDoF numerical models shall also be developed although it is desirable to use simplified ones like equivalent single-degree-of-freedom (SDoF) systems for large portfolios [5]. These complexities could make the FEMA P-58 methodology impractical for such cases, given a limited time/budget. Therefore, more simplified loss assessment procedures are typically sought to achieve a reasonable trade-off between accuracy and computational time/effort. For instance, the DVs of interest (*e.g.*, direct loss, repair time) can be measured at the building (global) rather than component (local) level. This is accomplished by using consequence models, which are the main focus of this study. Such models link the different global DSs a structure might experience due to ground shaking to the corresponding DV probability distributions [6]. Other approaches also exist, such as storey-loss functions [7], but they are outside the scope of this work.

Consequence models are conceptually applicable to any DV type, but this study focuses on direct loss (*i.e.,* from now on, referred to as "loss" for simplicity) and repair time. The consequence models for these DVs are termed damage-to-loss ratios (DLRs) and damage-to-repair time ratios (DTRs), respectively. DLRs link each structure-specific global DS to its respective loss ratio (repair costs normalised by the building replacement cost). Similarly, DTRs provide the repair time corresponding to each global DS divided by the total replacement time. It is critical to clarify that the DTRs here address solely the repair time (*i.e.,* the "rational" component) rather than total downtime, knowing that the former is the main constituent of the latter [8]. This is because the repair time reflects the duration required to repair physical damage, which is easier to estimate. Conversely, the "irrational" downtime component cannot be measured by the building's physical model as it is associated with financing and mobilisation, making it largely reliant on the local context (*e.g.,* bureaucracy). Nevertheless, the total downtime can be estimated by coupling DTRs with mobilisation/financing time models to address the irrational part [9].

Both DLRs and DTRs enable acquiring quick loss and repair-time estimates by combining them with building-level fragility relationships that define the probability of exceeding different structure-specific DSs given the ground-motion intensity. Fragility relationships are well-established and widely available for many building configurations and typologies [10]. They can also be derived via simplified approaches and models [11,12]. The main challenge, however, is related to the accuracy of the available DLRs/DTRs as they are among the largest -together with ground-motion variability- sources of uncertainty due to the difficulty in correlating structural and nonstructural damage to the corresponding loss and repair time [13]. Hence, care must be exercised in selecting

DLRs/DTRs to ensure the risk analysis reliability.

The derivation of DLRs usually stems from expert judgment or field observations of damaged buildings upon strong earthquakes [14–17]. While this approach appears the most trustworthy, numerous DLR models in the literature were derived based on limited empirical data [13]. The same applies to DTRs [6,18]. Furthermore, many DLR and DTR models are merely expressed as mean (expected) values without considering their significant variability. Alternatively, DLRs and DTRs can be derived numerically via approaches involving finite-element models and nonlinear response analysis. This has gained more popularity in the past few years, but only a few studies are available [8,13, 19], especially for Italian (and Mediterranean) building typologies.

To address the above limitations, this study demonstrates a practice-oriented simulation-based procedure that utilises direct loss (repair cost) and repair time estimates computed via the FEMA P-58 methodology to derive probabilistic models of DLRs and DTRs corresponding to user-defined building-level DSs. This procedure is applied for nine case-study reinforced-concrete (RC) frames with various heights, design-code levels, and plastic mechanisms, developed to reflect common residential RC buildings constructed during different eras in Italy and the Mediterranean region. Such frames serve as simplified archetype two-dimensional models for applications related to regional seismic-loss analysis. The derived DLRs and DTRs can be combined with fragility relationships to provide quick loss and repair-time estimates at the building's level consistent with those computed via the more robust FEMA P-58 methodology. The goodness-of-fit of the DLR and DTR distributions is assessed via the Kolmogorov-Smirnov (K–S) test [20]. This study also briefly looks at the possibility of correlating the repair times to direct loss for the case-study frames, which can be beneficial in evaluating the indirect loss resulting from downtime.

This paper is organised as follows: Section 2 presents the methodology used to derive the DLRs/DTRs and provides an explanation of damage, fragility, and loss assessments performed in this study. Section 3 defines the case-study frames with their structural/nonstructural components, plastic mechanisms, and DS mapping. Section 4 shows the nonlinear dynamic analysis and fragility/loss analysis results; it then derives DLR/DTR distributions for the case-study frames and briefly discusses correlating repair time to direct loss. Finally, Section 5 offers some remarks and conclusions.

## 2. Methodology

This study derives the statistical distribution of DLRs and DTRs via a numerical, simulation-based procedure, which includes the following steps as illustrated in Fig. 1: 1) define case-study buildings in terms of geometry, detailing, and material properties; 2) develop numerical models to simulate their nonlinear response; 3) run nonlinear static (pushover) analysis to map interstorey-drift ratio thresholds corresponding to the onset of different structure-specific DSs; 4) select hazard-consistent sets of ground motions and perform nonlinear time-history analysis (NLTHA); 5) use NLTHA results to derive building-level (global) fragility relationships; 6) define an inventory of structural and nonstructural components; 7) conduct a component-based risk assessment following the FEMA P-58 methodology; 8) characterise each DLR and DTR by fitting appropriate statistical distributions to the loss/repair time realisations resulting from step 7 after conditioning them on the global DS sustained by the structure. The following sub-sections shed some light on the definition of DSs, nonlinear analysis, fragility derivation, and loss assessment required by the proposed procedure.

### 2.1. Global damage states (DSs) and building-level fragility relationships

To characterise the various global damage conditions a building may experience due to earthquake-induced ground motion, four structure-specific DSs are defined as follows: DS1 (nonstructural damage due to infill cracking); DS2 (moderate damage of structural/nonstructural
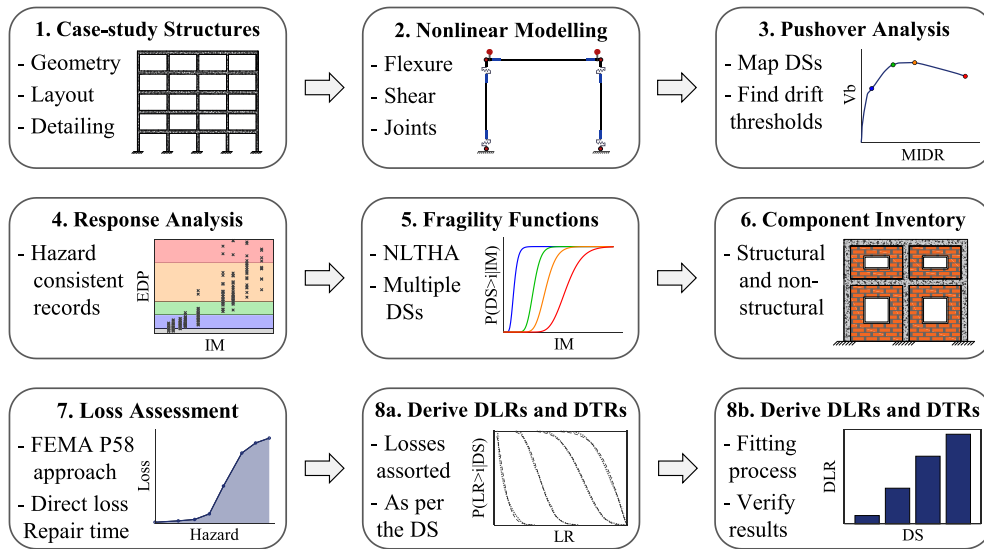
**Fig. 1.** Flowchart of the adopted methodology to derive the DLRs and DTRs.

components without significant yielding); DS3 (extensive damage, but the structure retains some residual strength and stiffness); DS4 (near-collapse conditions at which the strength and ductility of a structure are fully exploited, with deficient residual strength and stiffness). Each DS occurs when the structure attains a specific threshold expressed in terms of a suitable EDP. The EDP selected here is the maximum inter-storey drift ratio (MIDR); a reliable and widely-used proxy to measure global structural and nonstructural damage (at least for drift-sensitive components). The MIDR thresholds corresponding to the onset of DSs are calibrated by assessing the multi-level measurable criteria defined in Aljawhari et al. [21,22] via nonlinear static (pushover) analysis.

The potential of experiencing any of the above DSs during earthquakes is reflected by fragility relationships, which define the conditional probability of exceeding such DSs as a function of a ground-shaking intensity measure (IM), i.e., $P(DS \geq DSi|IM)$. These relationships can be derived via several approaches; many of them require performing NLTHAs using a set of ground-motion records, such as the cloud analysis [23] and incremental dynamic analysis [24]. This study specifically adopts the multiple-stripe analysis (MSA) approach [25], which is compatible with the FEMA P-58 methodology. The MSA subjects a building to multiple sets of ground-motion records with discrete IM values (i.e., stripes). MSA results can be subsequently utilised to derive building-level fragility relationships by fitting lognormal cumulative distribution functions (CDFs) via the procedure proposed by Baker [26], which relies on the maximum likelihood estimation. The fragility-relationship parameters for the "i-th" DS are the median ($\mu_{DSi}$) value and dispersion ($\beta_{DSi}$). Eq. (1) reports the mathematical form of these relationships, where $\Phi$ is the standard normal CDF.

$$P(DS \geq DSi|IM) = \Phi\left(\frac{\ln(IM/\mu_{DSi})}{\beta_{DSi}}\right) \qquad (1)$$

Each IM stripe in the MSA approach constitutes a site-specific hazard level, indicating that the selected record sets for analysis must be hazard-consistent. To ensure this consistency, records are selected/scaled to match a target conditional spectrum (CS) at each hazard level [27]. The CS defines the probability distribution of spectral accelerations over a range of vibration periods conditional on the spectral acceleration value(s) at a target conditioning period of interest (or range of periods) in addition to a specific rupture scenario.

### 2.2. Loss assessment and derivation of DLRs and DTRs

The PEER framework of risk analysis evaluates the mean annual

frequency ($\lambda$) of exceeding a selected DV (e.g., loss, downtime) as per Eq. (2). This framework integrates four stages: 1) hazard assessment, which determines the $\lambda$ values corresponding to various IM levels; 2) response analysis, that establishes the probabilistic distribution for relevant response parameters (i.e., EDPs) given the IM levels, $G(EDP|IM)$; 3) damage evaluation, in which a damage measure (DM), typically expressed as discrete DSs (see Section 2.1), is characterised based on the resulting EDPs. This is accomplished using fragility relationships/models defining the exceedance probability of different DSs. Fragility might be expressed as a function of the EDP or IM. The former applies to damage of individual building components, whereas the latter describes damage at the building level; 4) loss analysis, which computes the probability of exceeding any DV value conditional on the DM evaluated in stage 3. The outcome of this integration, $\lambda(DV)$, is deployed in the decision-making process following seismic risk assessments.

$$\lambda(DV) = \int\int\int G(DV|DM) \cdot dG(DM|EDP) \cdot dG(EDP|IM) \cdot d\lambda(IM) \qquad (2)$$

The FEMA P-58 methodology implements the PEER framework to evaluate losses and repair time (or any DV) via a component-based approach. It uses MSA results to derive joint statistical distributions for multiple EDPs (e.g., storey drifts, floor accelerations) at different IM levels. These distributions are then used to generate statistically-consistent sets of simulated demands (i.e., EDPs) at each IM level via Monte Carlo sampling. The simulated EDP sets are deployed to evaluate the DSs sustained by damageable components and convert them to loss/repair time by adopting suitable component fragility and consequence models. The losses/repair times experienced by such components are lastly aggregated to compute the overall building loss/repair time. Each simulated set of EDPs generates a single loss/repair time realisation. This process continues until producing a selected number of realisations. The loss/repair-time results are subsequently coupled with hazard information to estimate $\lambda$ for any loss/repair time value, i.e., $\lambda(DV)$.

Seismic loss can be also computed at a building's level to reduce computational time/effort, which is beneficial for risk assessments of large portfolios. This is usually performed by combining building-level fragility relationships with appropriate DLRs to generate vulnerability models that define the probability that the loss ratio exceeds a specific value given the IM level, $P(LR \geq lr|IM)$, as per Eq. (3). The second term, $P(LR \geq lr|DS = DSi)$, is the probability distribution of the DLR corresponding to the "i-th" global DS, which is the link between seismic loss to the global DS experienced by a building. The vulnerability models can be eventually coupled with hazard information, $\lambda(IM)$, to quantify the

mean annual frequency of exceeding any loss ratio value, $\lambda(LR \geq lr)$, as reported in Eq. (4). The same procedure can be applied to derive vulnerability models of repair time and estimate the $\lambda$ values for any repair-time ratio, $\lambda(TR \geq tr)$, simply by adopting DTRs instead of DLRs, *i. e.,* P($TR \geq tr|DS = DSi$), when applying Eqs. (3) and (4). Both the loss and repair time in Eqs. (3) and (4) are expressed as ratios, so they must be multiplied by the building replacement (reconstruction) cost and repair time, respectively, to obtain absolute numbers.

$$P(LR \geq lr|IM) = \sum_{i=1}^{n} P(LR \geq lr|DS = DSi)\cdot P(DS = DSi|IM) \quad (3)$$

$$\lambda(LR \geq lr) = \int_{\lambda} P(LR \geq lr|IM)\cdot d\lambda(IM) \quad (4)$$

The main aim of this study is to numerically derive distributions of DLRs and DTRs by adopting a simulation-based procedure that incorporates the following steps: 1) evaluate component-based seismic losses/repair times using the FEMA P-58 methodology; 2) condition the loss/repair time realisations on the corresponding global DS by comparing the set of EDPs simulated in each realisation with the thresholds corresponding to the onset of DSs. This allocates the realisations to a number of groups based on the global DS sustained by the building; 3) establish an empirical CDF (ECDF) for each group of loss/repair-time realisations obtained in the previous step; 4) for each ECDF of loss realisations, fit an adequate distribution that probabilistically characterises the DLR for a given global DS. A similar procedure is performed for the DTR distributions. Both DLRs and DTRs are statistically characterised via beta distributions [13,28]. The distribution parameters are the mean DLR and mean DTR corresponding to the "*i*-th" DS ($\mu_{DLRi}$ and $\mu_{DTRi}$), along with their coefficients of variation ($CoV_{DLRi}$ and $CoV_{DTRi}$). The shape parameters of the DLR beta distributions ($a_{DLRi}$ and $b_{DLRi}$) are computed using Eqs. (5) and (6). Similar parameters can be evaluated for the DTRs ($a_{DTRi}$ and $b_{DTRi}$) adopting the same equations.

$$a_{DLRi} = \frac{1 - \mu_{DLRi}}{CoV_{DLRi}^2} - \mu_{DLRi} \quad (5)$$

$$b_{DLRi} = \frac{a_{DLRi}(1 - \mu_{DLRi})}{\mu_{DLRi}} \quad (6)$$

## 3. Case-study application

### 3.1. Identification of case-study buildings

A sizable portion, equal to 29%, of the building stock in Italy consists of RC structures [29]. Most of these have a residential occupancy [30, 31]; hence, they are the main focus of this study. Such buildings vary in terms of height (number of storeys), but the vast majority are low-rise (up to three storeys), and mid-rise (four to seven storeys), whilst high-rise ones (more than eight storeys) are less common [31]. These buildings also differ based on the design-code level, which is a proxy for the age of construction, lateral-load-resisting systems, material properties, and detailing features.

To address the height variation, nine case-study RC frames are developed with three height categories, including 3-, 5-, and 8-storey frames representing low-, mid-, and high-rise buildings, respectively. The frames share a storey height of 3.0 m and consist of four bays with a length of 4.5 m in each horizontal direction (see Fig. 2). This simplifying assumption neglects the presence of structural irregularities and torsional response, making the developed frames unable to reflect the entire geometric variation of the Italian building stock. Nevertheless, these frames remain suitable for the aim of this study, *i.e.,* providing useful tools for portfolio-level risk analysis that typically utilises building archetypes. An archetype here refers to a simplified but representative model (*e.g.,* SDoF, two-dimensional MDoF) of a specific building typology, which captures the prevailing construction practices and

features (*e.g.,* materials, details). Such archetypes can be used to assess the seismic vulnerability of buildings of similar construction [32].

The frames vary as well in terms of design-code level. Specifically, the pre-code frames are designed to resist gravity loads only as per the 1939 Royal Decree n. 2229 in Italy [33]. A simulated design procedure is carried out to define the sizes and detailing of structural elements via the allowable stress design method [34]. The pre-code frames do not meet current seismic design provisions (*e.g.,* capacity-design rules, strong-column-weak-beam joints). Structural elements are poorly reinforced, and joints lack transverse reinforcement and proper anchorage [35], leading these frames to undergo a column-sway (soft storey) mechanism. Typical average values of material properties used in that era are adopted. The average concrete compressive strength ($f_{cm}$) is 16.5 MPa [36,37], and the average yield strength of rebar ($f_{ym}$) is 330 MPa [38,39]. The second group of case studies comprises high-code buildings designed based on the seismic provisions of Eurocode 8 [40] and the Italian National Code [41], adopting a design spectral acceleration of 0.083g and the detailing rules of high ductility class. A (global) beam-sway mechanism develops in these frames, in which plastic hinges form in beams and column bases, allowing a global ductile behaviour. $f_{cm}$ is 33 MPa and $f_{ym}$ is 490 MPa [42].

The last group of frames represents low-to-moderate-code structures (simply low-code hereinafter) built between the late 70s and 2008, *i.e.,* before introducing modern seismic design codes. During this period, a seismic classification took place in Italy in 1981 [14,31], and structural design requirements were upgraded, leading to improved performance of buildings in that era. Such performance remains, however, weaker than that of high-code buildings. The low-code frames are designed here by introducing weaknesses to the high-code case studies (*e.g.,* decreasing confinement and longitudinal rebar, reducing the size of some columns; [43]). The resulting low-code case-studies feature a mixed-sway mechanism combining joint failure with beam and/or column flexural hinging or shear failure. $f_{cm}$ is assumed 21 MPa [37] and $f_{ym}$ is 430 MPa [44]. Sample structural detailing is shown in Fig. 2b, which includes element sizes, longitudinal ($A_l$), and transverse reinforcement ($A_v$) for the columns identified by section A-A (see Fig. 2a).

RC frames in Italy, and the Mediterranean region, can be significantly influenced by the presence of masonry infills, which are deemed the major contributor to seismic losses [45,46]. Therefore, infills are explicitly considered in the design and numerical modelling. A uniformly-infilled configuration with double-leaf walls is assumed, which consists of 120 mm-thick external and 80 mm-thick internal clay bricks [47,48]. 2.0 m-wide and 1.25 m-high window openings are also assumed in the infill walls. The mechanical properties of the infill material are selected to represent those used in Italy and South-European countries [49,50]. The (average) compressive infill strength ($\sigma_m$) is equal to 2.40 MPa, the shear strength ($\tau_{m0}$) is 0.44 MPa, the sliding resistance ($\tau_m$) is 0.39, and the infill elastic modulus ($E_m$) is 2400 MPa. Each case-study frame is distinguished through an acronym specifying the number of storeys and design-code level, as explained in Table 1.

### 3.2. Nonlinear modelling strategy

The nonlinear response of the case-study buildings is simulated by developing two-dimensional numerical models using OpenSees [51]. Structural components are modelled as beam-column elements with finite-length plastic hinges to address the nonlinear flexural response, which is described via moment-curvature analyses [52,53]. The hysteretic response and post-capping degradation parameters are obtained from O'Reilly and Sullivan [54]. The shear failure is tackled by adding shear springs, in series, to the beam-column elements (see Fig. 3a). The parameters defining the shear backbone curve are acquired from Sezen and Moehle [3]. The post-capping shear response is defined per Mergos and Kappos [55] and Zimos et al. [56]. Joint shear failure is another brittle mechanism that may occur in pre-code frames, especially in
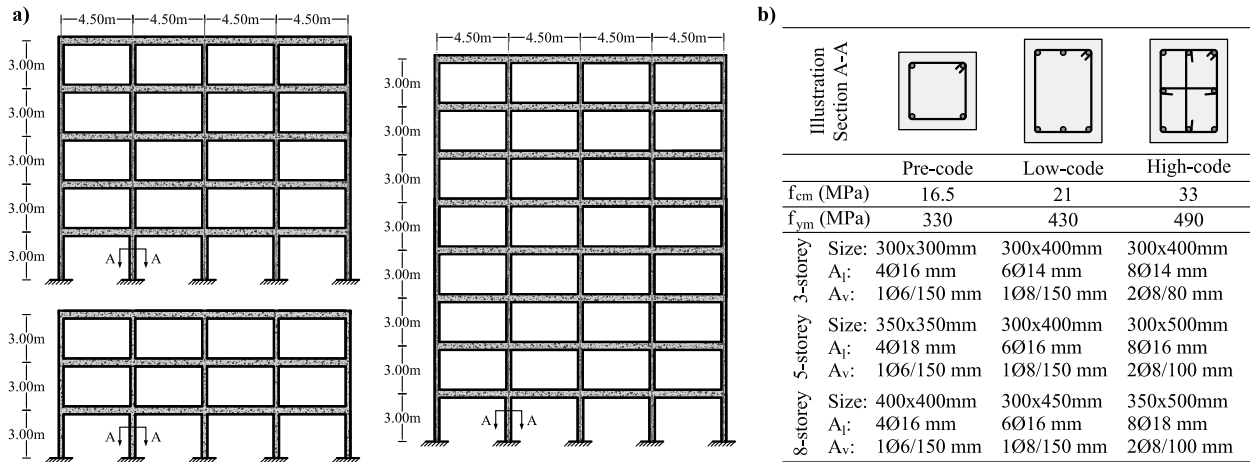
**Fig. 2.** a) layout of the case-study frames; and b) detailing for section A-A: $A_l$ is the longitudinal rebar, $A_v$ is the transverse rebar, and $\varnothing$ is the bar diameter.

**Table 1**
Acronyms identifying the developed case-study structures.

| Storey number/Code | Pre-code | Low-code | High-code |
|---|---|---|---|
| 3 Storeys | 3-Pre | 3-Low | 3-High |
| 5 Storeys | 5-Pre | 5-Low | 5-High |
| 8 Storeys | 8-Pre | 8-Low | 8-High |

external joints, so an additional spring is assigned in the beam-column joint zone (see Fig. 3b). The parameters of the joint nonlinear material are based on O'Reilly and Sullivan [54]. Floors are modelled as rigid diaphragms, and P-Delta effects are considered. Concrete degradation due to ageing effects like rebar corrosion [57–59] is not included for simplicity, although its consideration can improve the reliability of the analysis. This is a limitation of this study, but is consistent with the state-of-the-art practice of regional earthquake-loss modelling.

Infill walls are modelled as equivalent diagonal struts connecting between beam-column joints to address their effect on the global response of the frames. The force-deformation (backbone) relationship introduced by Liberatore and Decanini [49] and the hysteretic parameters calibrated by Mohammad Noh et al. [60] are assigned to the struts. Double struts are modelled in each direction to account for the increased shear demands due to local infill-frame interaction, following Burton and Deierlein [61], as seen in Fig. 3b. This strategy does not simulate the entire distribution of column shear due to frame-infill interaction, but it captures the shear demand increase in columns, allowing potential changes in the plastic mechanism. The effects of window openings on

the stiffness and lateral strength of infills are tackled by modifying the infill backbone curve as per Decanini et al. [62].

### 3.3. Inventory of structural and nonstructural components

The FEMA P-58 methodology requires defining a comprehensive inventory of fragility and consequence models for all damageable structural and nonstructural components. However, available models for the building stock in Italy (and the Mediterranean) are generally scarce. A common practice to tackle this issue is to compile an inventory from the FEMA P-58 component library developed explicitly for buildings in the USA, which might produce unreliable loss results if used for Italian buildings. It is also possible to convert USA-based losses to their European counterparts using the simplified factors proposed in Silva et al. [63]. However, such factors comprise high uncertainty as they require critical assumptions about the fractions of repair costs assigned to labour and materials, making them more applicable for approximate risk analysis. Therefore, this study attempts to adopt, whenever possible, component fragility and consequence models specific to Italian buildings to improve the reliability of loss estimates.

Accordingly, fragility models for structural components of the pre-code frames are acquired from Cardone [64], who calibrated them based on experimental testing of older Italian buildings. In contrast, fragility models for Italian low-code and high-code structural components are unavailable, so the default models in the FEMA P-58 guidelines, which correspond to ordinary and special RC frames, are adopted instead. This is deemed reasonable, assuming the seismic response of such components is similar to those used in Italy, given the similarity in
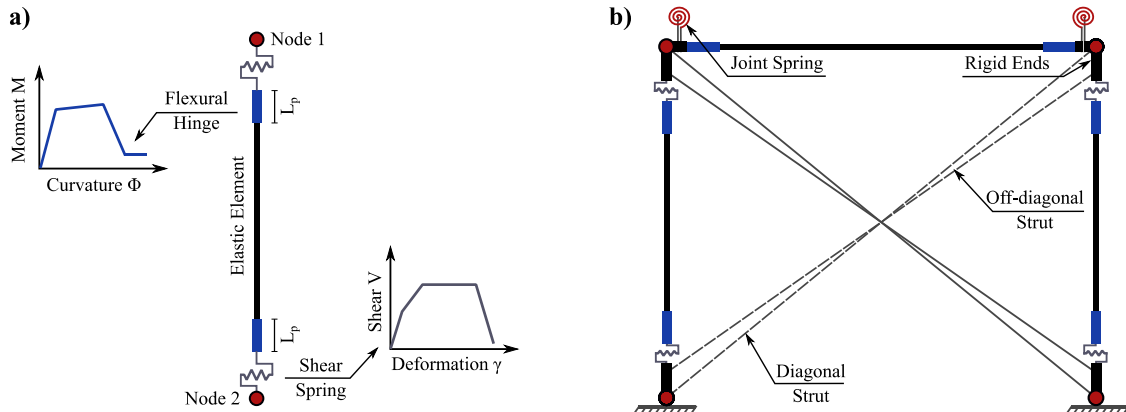


**Fig. 3.** a) modelling strategy for a column element; and b) modelling of an infilled frame configuration.

**Table 2**

Inventory of damageable structural and nonstructural components with their reference studies.

| Component Description | EDP | Unit | Reference |
|---|---|---|---|
| *RC structural components* | | | |
| External weak joints with end-hook longitudinal beam bars | IDR [%] | Each | • Fragility: Cardone [64]<br>• Repair cost: Cardone and Perrone [65]<br>• Repair time: Cardone et al. [9] |
| Internal joints with weak columns and beam flexural response | IDR [%] | Each | • Fragility: Cardone [64]<br>• Repair cost: Cardone and Perrone [65]<br>• Repair time: Cardone et al. [9] |
| Brittle weak and short RC columns | IDR [%] | Each | • Fragility: Cardone [64]<br>• Repair cost: Cardone and Perrone [65]<br>• Repair time: Cardone et al. [9] |
| ACI 318 OMF with weak joints and beam flexural response, column and beam 24" × 24", beam one side[a] | IDR [%] | Each | • Fragility: FEMA [4]<br>• Repair cost: Cardone and Perrone [65]<br>• Repair time: Cardone et al. [9] |
| ACI 318 OMF with weak joints and beam flexural response, column and beam 24" × 24", beam two sides[a] | IDR [%] | Each | • Fragility: FEMA [4]<br>• Repair cost: Cardone and Perrone [65]<br>• Repair time: Cardone et al. [9] |
| ACI 318 SMF, column and beam 24" × 24", beam one side[b] | IDR [%] | Each | • Fragility: FEMA [4]<br>• Repair cost: Cardone and Perrone [65]<br>• Repair time: Cardone et al. [9] |
| ACI 318 SMF, column and beam 24" × 24", beam two sides[b] | IDR [%] | Each | • Fragility: FEMA [4]<br>• Repair cost: Cardone and Perrone [65]<br>• Repair time: Cardone et al. [9] |
| *Nonstructural components* | | | |
| Masonry infill walls and partitions composed of hollow clay bricks | IDR [%] | m$^2$ | • Fragility: Del Gaudio et al. [47]<br>• Repair cost: Del Gaudio et al. [47]; Cardone and Perrone [66]<br>• Repair time: Cardone et al. [9] |
| Services embedded within masonry infill walls/partitions: electric systems, HVAC, plumbing, floor/wall tiling | IDR [%] | m$^2$ | • Fragility: Del Gaudio et al. [47]<br>• Repair cost: De Risi et al. [48]; Cardone and Perrone [66]<br>• Repair time: Cardone et al. [9] |

[a] OMF: Ordinary moment-resisting frame.
[b] SMF: Special moment-resisting frame.

design methods and reinforcement details. The repair-cost consequence models for all the previous structural components are defined following Cardone and Perrone [65], who relied on the 2013 price list for public works in the Basilicata region in Italy. Nonstructural components include masonry infills. Their fragility models are obtained from Del Gaudio et al. [47], who derived them based on experimental tests. The repair-cost consequence models are acquired from the same study. However, only average repair costs are provided for each DS. Therefore, the dispersion coefficients found in Cardone and Perrone [66] are assigned to these average values to account for uncertainties.

Both structural components and infills are drift sensitive. Other components, mainly related to services (*e.g.,* electrical/plumbing systems, radiators, heaters), are sensitive to floor accelerations. However, these services might also be embedded within infills; a common practice in RC residential buildings in Italy (and the Mediterranean), which makes it possible to correlate the damage of services to that sustained by infills. This means that the fragility models of infills can simultaneously characterise the damage of services [48,65]. De Risi et al. [48], derived the repair-cost consequence models for services, validating them against post-event damage/loss data from the 2009 L'Aquila earthquake in Italy. These models are used here, but the repair costs are expressed as average values only, so the dispersion coefficients of Cardone and Perrone [66] are adopted again. A few other acceleration-sensitive components, like chandeliers, are not embedded within infills. These are disregarded here due to their minor contribution to the overall seismic losses and lack of fragility/consequence models specific to Italy. Table 2 summarises all the selected building components, along with their reference studies and EDPs.

Unlike repair costs, the literature has not well-established consequence functions of repair times for Italian building components. However, Cardone et al. [9] heuristically derived such functions for structural components and infills (with embedded services) based on local manuals of civil engineering works in Italy. Despite the high

uncertainties behind these functions, Cardone et al. [9] used them to estimate the repair times for several structures that matched empirical values acquired from local contractors. Therefore, such functions are adopted in this study (see Table 2). The dispersion coefficients are estimated by taking the square root of the sum of squares of the dispersions used for the repair-cost consequence functions and 0.25 [4]. Building contents (*i.e.,* furnishings) are not addressed as part of the inventory [67] due to the lack of fragility/consequence models specific to Italian buildings, which indicates that the defined component inventory is not exhaustive. Nevertheless, most losses are attributed to infills and services [17,68] rather than building contents [69], making the assumptions adopted here reasonable. Furthermore, content losses might be irrelevant given the residential use of the case-study frames, especially since they do not contain special equipment like those found in hospitals, factories, and educational facilities [6].

*3.4. Dynamic characteristics and mapping of DS thresholds*

To understand the performance and verify the plastic mechanism of the case-study structures, an initial assessment is conducted using nonlinear static (pushover) analysis. The MIDR thresholds corresponding to the onset of the global DSs are also calibrated using pushover analysis based on Section 2.1. Fig. 4 depicts the pushover curves and the mapped MIDR thresholds for all DSs. It is noted that the improvement in design-code levels and plastic mechanisms corresponds to an enhancement of lateral strength/stiffness. The thresholds of structural DSs, especially those relying on the ductility of structural elements (*i.e.,* DS3 and DS4), notably improved. Fig. 5 shows the resulting plastic mechanisms measured at DS4. The high-code frames experience a global-sway mechanism, while the pre-code ones show a column-sway (soft-storey) behaviour. The low-code frames exhibit a mixed-sway mechanism combining multiple hinging patterns. The dynamic characteristics of the frames, including the fundamental (first mode) period of vibration (T$_1$)
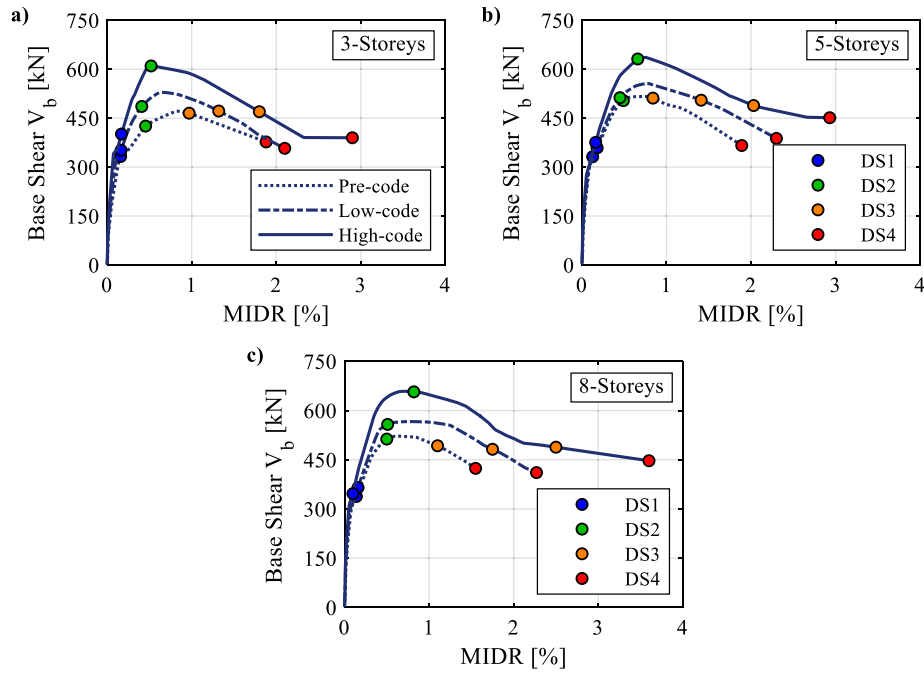
**Fig. 4.** Pushover curves and DS thresholds for the: a) 3-storey; b) 5-storey; and c) 8-storey frames.
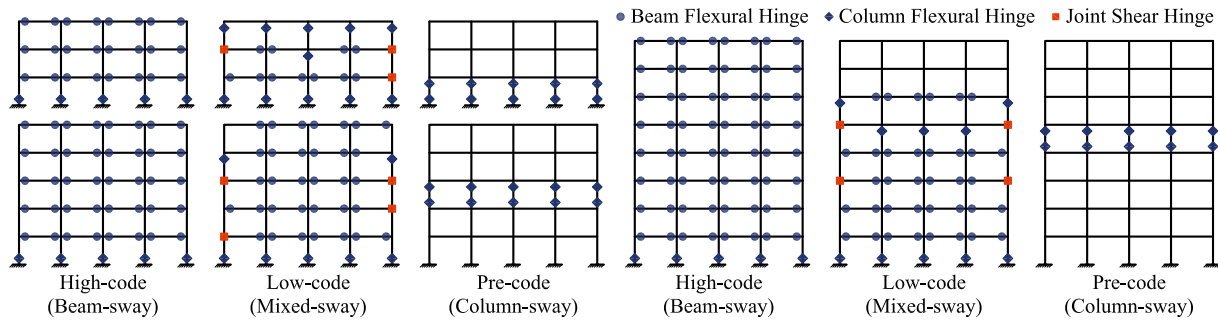


**Fig. 5.** Schematic illustration of the plastic mechanisms for all case-study frames.

**Table 3**
Dynamic characteristics of the case-study structures.

| Building/property | 3-Pre | 3-Low | 3-High | 5-Pre | 5-Low | 5-High | 8-Pre | 8-Low | 8-High |
|---|---|---|---|---|---|---|---|---|---|
| First-mode period, $T_1$ [s] | 0.33 | 0.27 | 0.22 | 0.46 | 0.39 | 0.34 | 0.66 | 0.61 | 0.53 |
| Mass participation [%] | 93.7 | 94.2 | 95.1 | 89.0 | 89.5 | 91.3 | 85.3 | 86.7 | 87.2 |

and mass participation ratio, are reported in Table 3.

### 3.5. Seismic hazard analysis and record selection

The dynamic performance of the case-study frames is assessed via MSA. This requires characterising the site hazard to estimate the frequency at which different IM levels might be exceeded, followed by ground-motion record selection. The IM selected to measure the ground shaking intensity is the geometric mean of the 5%-damped spectral acceleration values over a specific range of periods (avgSa). avgSa accounts indirectly for the effects of higher modes and period elongation due to strength/stiffness degradation [70]. Compared to conventional IMs like the spectral acceleration at $T_1$, i.e., Sa($T_1$), avgSa has a higher relative sufficiency and can minimise response variability [71]. avgSa is calculated considering ten equally-spaced periods ranging between $0.2T_1$ and $1.5T_1$ [72]. The $T_1$ values used to define the period ranges are those

resulting when infills are disregarded, i.e., assuming bare-frame configurations [21], to address the increased elongation associated with the loss of stiffness and strength upon infill damage [73].

Moreover, the same period range is used to define avgSa for the case-study frames with the same height category in lieu of assigning a different range for each frame. This enables a direct comparison between the frames with a similar number of floors in terms of their

**Table 4**
Fundamental periods $T_1$ and period ranges selected to define avgSa.

| Height category/ Property | 3-storey Frames | 5-storey Frames | 8-storey Frames |
|---|---|---|---|
| $T_1$ used for each period range | 0.94s | 1.34s | 1.80s |
| Symbol for avgSa and period range | avgSa(0.19 – 1.40s) | avgSa(0.27 – 2.00s) | avgSa(0.36 – 2.70s) |

fragility and seismic performance. It also reduces the iterations of hazard analysis and ground-motion selection. The $T_1$ values adopted to compute the period ranges are those associated with the pre-code configurations (*i.e.*, 3-Pre, 5-Pre, and 8-Pre frames), as shown in Table 4.

Upon defining the IMs, site-specific seismic hazard analysis is conducted, assuming the case-study frames are located in L'Aquila (42.3498 N°, 13.3995 E°); among Italy's highest seismically active areas. A soil type C with a shear-wave velocity of 270 m/s is assumed to address seismic wave amplification. The hazard is analysed via Open-Quake Engine, an open-source tool developed by the Global Earthquake Model Foundation [74], adopting the 2013 Euro-Mediterranean Seismic Hazard Model [75]. The standard deviation for avgSa prediction is computed using the Baker and Jayaram [76] correlation model, which is applied to all ground-motion models (GMMs) in the logic tree except for the Akkar and Bommer GMM [77], where the European correlation model of Akkar et al. [78] is adopted. Next, 14 discrete IM levels reflecting different return period ($T_r$) values ($T_r = 1/\lambda$) are defined (30, 45, 75, 100, 200, 475, 712, 975, 1463, 2475, 3670, 4975, 7475, and 9975 years). Hazard disaggregation is then performed to specify the magnitudes ($M_w$) and distances with the highest hazard contribution. For simplicity, only the branch with the largest weight in the logic tree is included, which corresponds to the area source model and GMMs developed by Akkar and Bommer [77], Faccioli et al. [79], and Zhao et al. [80].

For each IM level, a set of 35 ground motions are selected from the NGA-West2 database [88]. To assure hazard consistency, the records are scaled to match the target CS associated with every IM value and its hazard level (*i.e.*, $T_r$). In this study, simplified CSs are established to characterise the probability distribution of spectral accelerations at various vibration periods conditional on: 1) a target avgSa value defined from hazard analysis; and 2) a specific rupture scenario including the mean $M_w$ and Joyner-Boore source-to-site distance ($R_{jb}$) acquired from hazard disaggregation. The Akkar and Bommer GMM [77], which is the most suitable for dominant earthquakes in the tectonic regime of interest, is applied to estimate IM levels. The generation of target CSs and subsequent record selection is carried out using the EzGM tool; an open-source algorithm [81]. Record linear scaling, up to a scaling factor of 2.5, is permitted to match the target CSs. Fig. 6a illustrates the hazard curves defining avgSa values and their corresponding $\lambda$. Fig. 6b shows the mean CS at a 975-year $T_r$, conditional on avgSa(0.19 − 1.40s) and the (individual) spectra of the selected records. The mean CS and record spectrum ($\pm$ two standard deviations, $\sigma$) are also displayed. The remaining record-selection results are not shown for brevity.
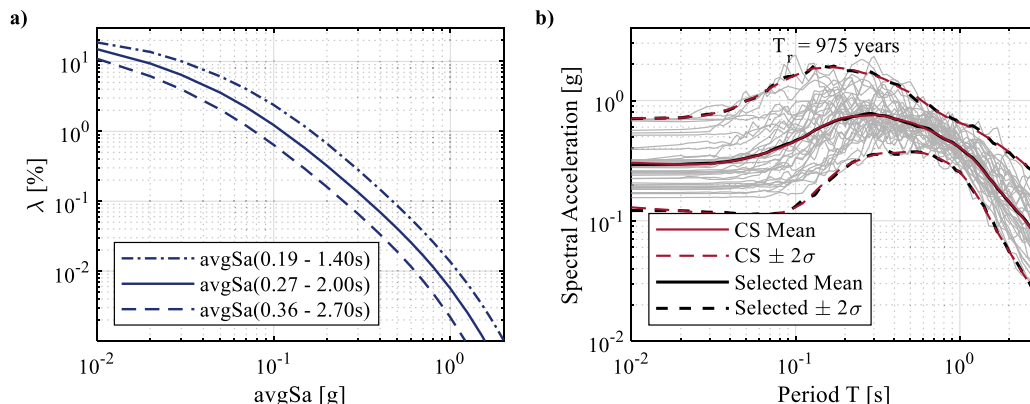
## 4. Analysis results and discussion

### 4.1. MSA and building-level fragility relationships

MSA is carried out using the selected records to assess the seismic performance of the case-study frames. As expected, the pre-code frames show the weakest response. Such results are depicted in Fig. 7, which provides the MSA results for the 5-storey frames. Fig. 7a indicates that the 5-Pre frame exhibits a significant number of analysis cases with high DSs, even at low IM levels. This frame remained undamaged in less than 7% of the cases and experienced DS1 in almost 25%. DS2 and DS3 account for 21% of the analysis cases, whereas 47% are either DS4 or collapse. Collapse corresponds here to the instability of numerical analyses (decided upon testing multi-criteria convergence algorithms) and/or excessive MIDR values larger than a nominal threshold (*e.g.*, drifts beyond DS4 causing severe strength degradation during pushover analysis). The 5-Low frame showed a slightly better performance (see Fig. 7b). Specifically, the frame was undamaged in 12% of the cases and acquired DS1 in 21%. DS2 and DS3 comprise 32%, while DS4 and collapse account for 35%. Lastly, Fig. 7c shows that the 5-High frame remained undamaged in 14% of the analysis cases and reached DS1 in 26%. DS2 and DS3 were experienced in 38% of the cases, whereas only 22% are either DS4 or collapses. Similar observations could be recorded regarding the 3- and 8-storey frames.

The MSA results are subsequently adopted to derive building-level fragility relationships for the case-study frames (see Fig. 8) using the procedure of Baker [26]. The median and dispersion values, *i.e.*, $\mu_{DSi}$ and $\beta_{DSi}$, for all DSs are reported in Table 5. Fig. 8 proves that the fragility relationships improve (*i.e.*, shift towards the right) when the plastic mechanism and design-code level are enhanced. This is not very evident in the DS1 fragility relationships as they are mainly associated with the initial cracking of infills, which takes place before any structural damage. In contrast, the right-shift of fragility relationships becomes significant for higher DSs (*e.g.*, DS3 and DS4) as they depend on the structure's performance under high levels of nonlinear deformation.

### 4.2. Loss analysis using the FEMA P-58 methodology

Seismic losses are now estimated following the FEMA P-58 methodology and using the Performance Assessment Calculation Tool (PACT) [4] to run calculations. A building performance model is assembled in PACT for each case-study frame considering the component inventory defined in Section 3.3. PACT first requires defining the replacement costs for all case studies, which are based on the average construction price per unit area for residential buildings in Italy. This is equal to €900/m² , including construction, demolition, and disposal [65]. Such value does not cover building contents, in line with the assumptions listed in Section 3.3. It should be noted that the adopted replacement
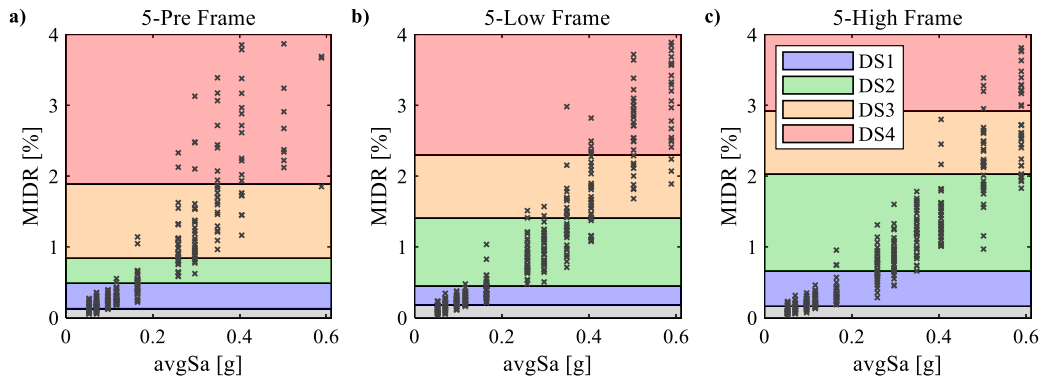


**Fig. 6.** a) hazard curve for avgSa; and b) CS and spectra of selected records for avgSa(0.19 − 1.40s) at $T_r$ of 975 years.

**Fig. 7.** MSA results and their DS classification for the: a) 5-Pre frame; b) 5-Low frame; and c) 5-High frame.
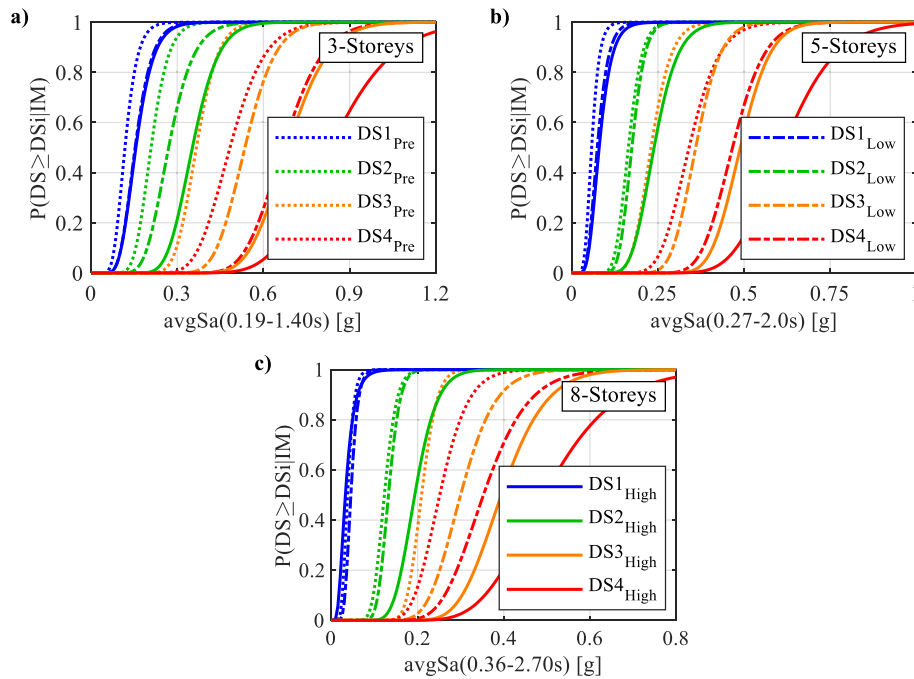


**Fig. 8.** Fragility relationships for the: a) 3-storey frames; b) 5-storey frames; and c) 8-storey frames.

**Table 5**
Median $\mu_{DSi}$ and dispersion $\beta_{DSi}$ values for all fragility relationships.

| DS/Frame | $\mu_{DS1}$ [g] | $\beta_{DS1}$ | $\mu_{DS2}$ [g] | $\beta_{DS2}$ | $\mu_{DS3}$ [g] | $\beta_{DS3}$ | $\mu_{DS4}$ [g] | $\beta_{DS4}$ |
|---|---|---|---|---|---|---|---|---|
| 3-Pre | 0.118 | 0.291 | 0.209 | 0.230 | 0.367 | 0.164 | 0.484 | 0.199 |
| 3-Low | 0.154 | 0.300 | 0.270 | 0.253 | 0.536 | 0.158 | 0.669 | 0.165 |
| 3-High | 0.156 | 0.308 | 0.353 | 0.205 | 0.685 | 0.164 | 0.834 | 0.205 |
| 5-Pre | 0.058 | 0.305 | 0.164 | 0.192 | 0.230 | 0.202 | 0.340 | 0.204 |
| 5-Low | 0.074 | 0.336 | 0.174 | 0.175 | 0.360 | 0.159 | 0.466 | 0.159 |
| 5-High | 0.080 | 0.355 | 0.239 | 0.227 | 0.489 | 0.142 | 0.613 | 0.195 |
| 8-Pre | 0.037 | 0.305 | 0.123 | 0.183 | 0.209 | 0.135 | 0.251 | 0.205 |
| 8-Low | 0.045 | 0.282 | 0.132 | 0.159 | 0.300 | 0.210 | 0.353 | 0.230 |
| 8-High | 0.032 | 0.489 | 0.194 | 0.209 | 0.394 | 0.205 | 0.494 | 0.256 |

costs and component consequence functions reflect the prices in Italy in 2014, which have been increasing since then due to currency inflation. This is not tackled here as the replacement costs of the case-study frames normalise all seismic loss results. Uncertainties related to component modelling are accounted for by considering a modelling dispersion of 0.3, as the FEMA P-58 guidelines [4] recommend.

PACT also requires selecting a loss threshold above which the building will likely be demolished and replaced instead of being repaired. This threshold is typically between 40% and 60% of the replacement cost, which may produce numerous realisations with losses equal to the replacement cost, especially at large IM levels. This introduces bias in deriving DLRs for high DSs (*e.g.*, DS3-DS4) as they become closer to 1.0. Hence, this threshold is set as 100%. The collapse potential is addressed in PACT by assigning collapse fragility relationships. The possibility of sustaining large residual (permanent) drifts that make the structure irreparable is tackled as well by using a repairability
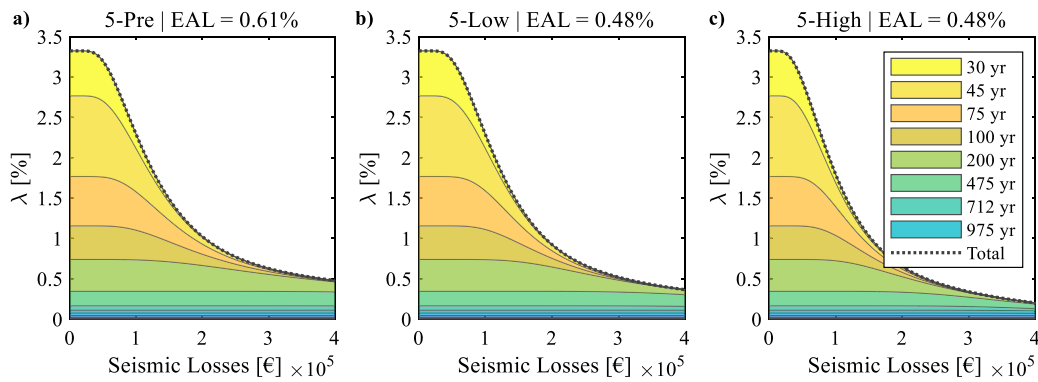
**Fig. 9.** Loss curves with contributions of various hazard levels for the: a) 5-Pre; b) 5-Low; and c) 5-High frames.
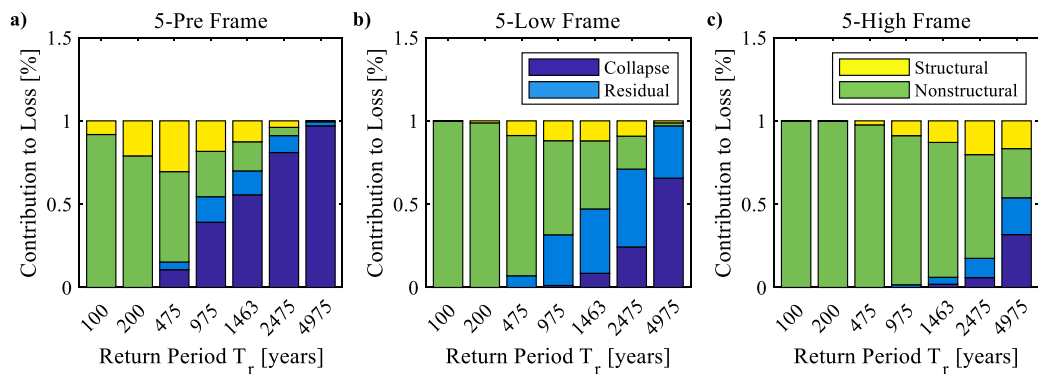


**Fig. 10.** Loss disaggregation at different hazard levels for the: a) 5-Pre; b) 5-Low; and c) 5-High frames.

fragility relationship with a median residual drift ratio of 0.01 and a dispersion of 0.3 [4]. The analysis is run considering 1000 loss realisations at each IM level. This number is selected upon conducting sensitivity checks to ensure that the loss results and derived DLRs are numerically stable.

Fig. 9 shows the loss curves describing the $\lambda$ values for a range of seismic losses, and the contribution of individual hazard levels for the 5-storey frames. The expected annual loss (EAL), computed by integrating losses over all hazard levels, is also reported in Fig. 9 to provide an indicator of the average losses incurred on a yearly basis. As expected, the EAL values demonstrate that the 5-High frame incurs the least losses, unlike the 5-Low and 5-Pre frames. It is also shown that low hazard levels contribute most to the EAL values due to their higher rates of occurrence. The resulting EALs, however, are generally lower than expected as the replacement threshold is set as 100%. If the threshold is changed to 40% [4], the EAL values would considerably increase and reach 0.5% for the 5-High, 0.60% for the 5-Low, and 0.82% for the 5-Pre frames. The obtained EALs are consistent with other studies assessing losses for Italian RC buildings [65,82].

Fig. 10 shows the relative contribution of structural/nonstructural damage, collapse, and large residual drifts to the resulting losses at different hazard levels for the 5-storey frames. Nonstructural damage dominates the losses at low hazard levels, whilst losses at high hazard levels are primarily attributed to structural collapse and excessive residual drifts. The contribution of collapse and excessive residual drifts for the 5-Pre frame is evident at $T_r$ values as low as 475 years (Fig. 10a). Conversely, this contribution becomes noticeable starting from $T_r$ values of 975 and 1463 years for the 5-Low and 5-High frames, respectively (see Fig. 10b–c). Lastly, the contribution of structural components at low $T_r$ values $\leq 475$ years is considerable solely in the 5-Pre case, while it is almost negligible in the other two. This is because the 5-Pre frame includes brittle structural components that experience large damage, even against minor ground shaking with low $T_r$ values, unlike the more

ductile 5-High and 5-Low frames.

### 4.3. Derivation of structure-specific DLRs

DLRs are now derived utilising the FEMA P-58 loss results. All loss realisations are first conditioned on the corresponding global DSs attained by the case-study frames. This is accomplished by investigating the drift demands simulated by PACT at each realisation and then finding the maximum value across different storeys (*i.e.,* simulated MIDR). Next, the simulated MIDRs are compared to the DS thresholds in Fig. 4 to allocate each realisation to a suitable global DS. This process divides these realisations into four sets; each one is conditioned on a particular DS. An ECDF is subsequently assembled for every individual set. The DLRs are finally derived by fitting a beta distribution to each ECDF, which statistically characterises seismic losses given the global DS. Other distributions (*e.g.,* Weibull, lognormal, uniform) are also tested for comparison purposes. The loss analyses performed to derive the DLR distributions disregard both collapse and excessive residual drift cases. This is because the DSs associated with the DLRs (and DTRs) rely on the assumption that the structure has not collapsed.

An example is offered in Fig. 11a, where the ECDFs and fitted beta distributions are plotted for the 5-Pre frame. The horizontal axis is the loss ratio, LR, and the vertical axis is the probability of exceeding any loss-ratio value given that the building is in the "*i*-th" DS, *i.e.,* $P(LR \geq lr|DS = DSi)$. Both the ECDFs and fitted beta distributions appear consistent, at least from a visual standpoint. Further confirmation of the fitted distributions is provided in Fig. 11b, which compares the normalised loss realisations from PACT at different IM levels and the vulnerability function, which expresses the LR as a function of the IM. This function is simply generated by combining the derived DLRs with the corresponding building-level fragility relationships using Eq. (3). Fig. 11b shows that the mean LRs obtained from PACT at each IM level are almost identical to those estimated by the vulnerability function,
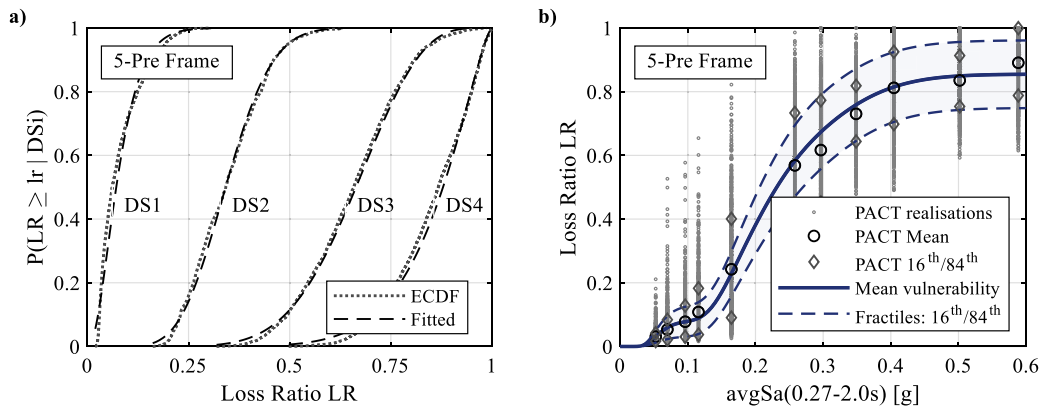
**Fig. 11.** a) ECDFs and beta distributions of the DLRs for the 5-Pre frame; and b) vulnerability function evaluated using the derived DLRs in comparison with loss realisations produced by PACT for the 5-Pre frame.

with solely a slight deviation not exceeding 7% at a few IM levels. Comparable remarks are also deduced regarding the $16^{th}/84^{th}$ fractiles. Similar observations are recorded for the remaining case-study frames but are not shown for brevity.

The matrix summarising the DLR distribution parameters for all case-study frames is reported in Table 6, including the mean and coefficient of variation ($\mu_{DLRi}$ and $CoV_{DLRi}$). An illustration of the $\mu_{DLRi}$ values with $\pm$ 1$\sigma$ error bars is also provided in Fig. 12. It is noted that for the same number of storeys, the $\mu_{DLRi}$ values for the high-code frames are the largest compared to the low-code and pre-code counterparts, which might be attributed to their plastic mechanism. Specifically, the high-code frames exhibit a beam-sway mechanism that enables uniform distribution of nonlinear deformations across different storeys, with more structural/nonstructural components deforming. This leads to more damaged components and, eventually, higher losses. In contrast, nonlinear deformations in the pre-code frames are concentrated on a specific floor due to their column-sway mechanism, making the components on other floors undergo small deformations or even remain elastic. Hence, the number of damaged components and resulting $\mu_{DLRi}$ values become lower. For instance, the difference in $\mu_{DLRi}$ values between the high-code and pre-code frames with the same number of storeys reaches up to 32% for DS1 and up to 11% for the other DSs.

For the frames with the same design-code levels, the $\mu_{DLRi}$ values are generally the largest for the 3-storey frames, followed by the 5- and 8-storey frames, respectively. This is because the losses are normalised by higher replacement costs in the frames with a larger number of storeys. Moreover, the upper floors in such frames might experience small deformations only, which limits the extent of damage and leads to lower $\mu_{DLRi}$ values. Accordingly, a difference of up to 25% is observed in the $\mu_{DLRi}$ values of DS1 between the 3- and 8-storey frames with the same design code. The difference reduces to 11% for the other DSs. Lastly, it is noted that the $CoV_{DLRi}$ values for low DSs (DS1 and DS2), are remarkably larger than those for DS3 and DS4. This is attributed to the large vari-

ability of structural response and the corresponding loss realisation at low IM levels,which govern the derivation of DLR distributions of DS1 and DS2 [13,15].

Despite the variation of $\mu_{DLRi}$ values among the frames with various heights and design codes, the difference for most DSs is not significant. This is because the estimated losses and derived DLRs are dominated by the damage of nonstructural components and services, which experience high DSs and losses even at low ground shaking, irrespective of the building height and design code. If the loss analyses conducted here included structural components only, the difference in DLRs would be more remarkable between multiple heights/design-code levels. To prove this statement, Fig. 13 compares the $\mu_{DLRi}$ values for DS2 to DS4 between the 5-Pre and 5-High frames, disregarding infills and services in both structural analysis and loss assessment. DS1 is not considered as it is related to the initial cracking of infills rather than structural damage. It is observed that the $\mu_{DLRi}$ values for the 5-High frame are 28%–35% larger than those associated with the 5-Pre frame.

### 4.4. Repair-time analysis using the FEMA P-58 methodology and derivation of structure-specific DTRs

Repair times are now computed via PACT, based on the FEMA P-58 methodology. PACT first requires the maximum number of workers who can simultaneously work inside the building. Due to the lack of any guidance/reference for the Italian buildings, the value recommended by the FEMA P-58 guidelines [4] is used; equal to 0.001 workers per square foot ($\approx$ 1 worker/92 m$^2$). The replacement time for each case-study frame is quantified by aggregating the repair times needed to reconstruct all individual components adopting the appropriate consequence functions discussed in Section 3.3 and assuming the selected maximum number of workers. The resulting replacement-time values are 198, 330, and 528 days for the 3-, 5-, and 8-storey frames, respectively. These values are consistent with empirical data from contractors after the 2009

**Table 6**
Mean $\mu_{DLRi}$ and coefficient of variation $CoV_{DLRi}$ values for the DLRs of all case-study structures.

| DS/Frame | DS1 | | DS2 | | DS3 | | DS4 | |
|---|---|---|---|---|---|---|---|---|
| | $\mu_{DLR1}$ [%] | $CoV_{DLR1}$ | $\mu_{DLR2}$ [%] | $CoV_{DLR2}$ | $\mu_{DLR3}$ [%] | $CoV_{DLR3}$ | $\mu_{DLR4}$ [%] | $CoV_{DLR4}$ |
| 3-Pre | 11.3 | 0.275 | 36.4 | 0.322 | 65.6 | 0.182 | 82.3 | 0.166 |
| 3-Low | 12.5 | 0.320 | 36.6 | 0.283 | 68.0 | 0.154 | 90.9 | 0.088 |
| 3-High | 14.8 | 0.361 | 37.7 | 0.277 | 73.8 | 0.139 | 92.0 | 0.071 |
| 5-Pre | 10.9 | 0.366 | 32.2 | 0.242 | 62.2 | 0.197 | 84.6 | 0.129 |
| 5-Low | 11.3 | 0.287 | 35.5 | 0.271 | 63.8 | 0.165 | 87.2 | 0.116 |
| 5-High | 12.9 | 0.397 | 36.5 | 0.263 | 68.4 | 0.135 | 88.7 | 0.099 |
| 8-Pre | 10.0 | 0.362 | 34.9 | 0.314 | 59.9 | 0.180 | 78.9 | 0.172 |
| 8-Low | 10.5 | 0.350 | 36.2 | 0.290 | 61.5 | 0.180 | 82.9 | 0.164 |
| 8-High | 11.9 | 0.508 | 38.4 | 0.268 | 66.6 | 0.138 | 84.6 | 0.119 |
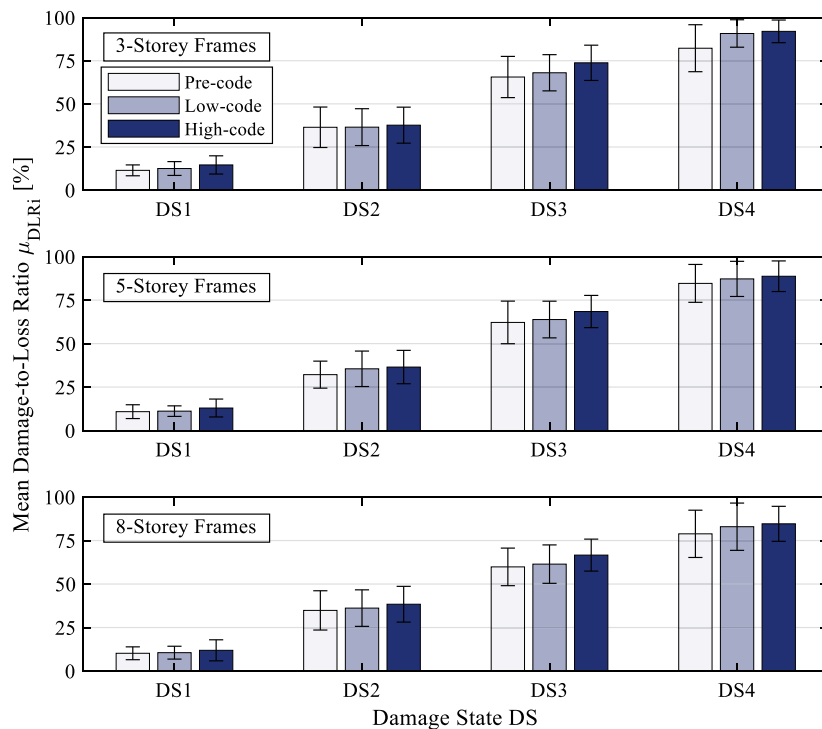
**Fig. 12.** Bar charts for the mean DLR values ($\mu_{DLRi}$) and error bars of $\pm1\sigma$ for all the case-study frames.
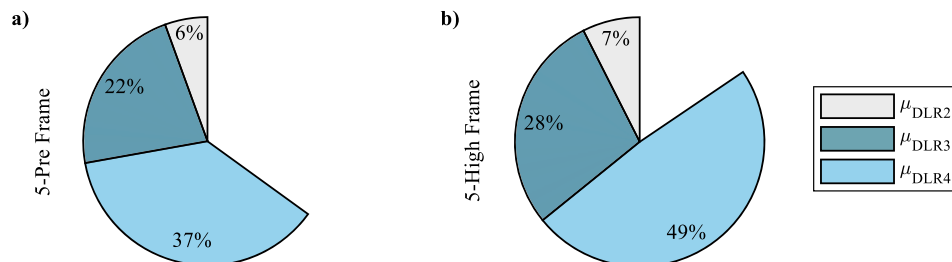


**Fig. 13.** $\mu_{DLRi}$ values assuming the absence of infills and services for the: a) 5-Pre frame; and b) 5-High frame.

L'Aquila earthquake in Italy [9].

The repair-time estimation via PACT involves some limitations. First, this repair time considers only the duration needed to achieve a full recovery upon seismic damage. Other useful recovery states, such as re-occupancy and functional recovery [83], are not addressed. It is also assumed that the working force depends on the floor area rather than the damage extent, which may not always be rational [84]. Moreover, repair strategies are considered either in serial or parallel fashions. The former assumes a sequential repair across different floors, and the latter deems the repair to co-occur on all floors. These assumptions may not correspond to real-life repair-sequencing strategy, but they could at least serve as upper/lower bounds of the actual repair time. As an example, Fig. 14 shows the repair times per floor for the 5-Pre frame in one of the realisations at the hazard level with a 712-year $T_r$, considering parallel and in-series repair-sequencing strategies. The contributions of different components are also depicted. The overall repair time resulting from the former strategy is 72 days, whereas the latter produced a 200-day repair time. It is critical to recall that the repair times computed here represent only the "rational" part of the full downtime pertaining to the duration required to perform repair works. The full downtime, on the other hand, might be remarkably larger due to delays related to financing, mobilisation, and procurement.

The repair times resulting from PACT are then deployed to derive DTRs using the same procedure adopted earlier for the DLRs. Fig. 15a

shows the ECDFs and fitted beta distributions representing the DTRs for the 5-Pre frame. The horizontal axis is the repair-time ratio, TR, and the vertical axis is the probability of exceeding any repair-time ratio value given the building is in the "$i$-th" DS, $i.e.$, $\mathrm{P}(TR \geq tr | DS = DSi)$. Fig. 15b compares the repair-time realisations obtained via PACT at different IM levels for the 5-Pre frame and the repair-time vulnerability relationship (mean and $16^{th}/84^{th}$ fractiles), defining TR as a function of IM. This function is derived by combining the DTRs of the 5-Pre frame with its building-level fragility relationships via Eq. (3). A high consistency is observed between the TR values estimated by the vulnerability function and those generated by PACT. Both the repair-time results and derived DTRs assume a sequential repair strategy, which represents an upper bound for the repair time associated with each DS. This strategy is relatively conservative but remains more realistic than the parallel one, where all floors undergo repair works simultaneously. The DTR distribution parameters ($\mu_{DTRi}$ and $CoV_{DTRi}$) are reported in Table 7 for each case-study frame. The $\mu_{DTRi}$ values with $\pm1\sigma$ error bars can be also visualised in Fig. 16.

### 4.5. Goodness-of-fit for the derived DLR and DTR distributions

The goodness-of-fit of the derived DLR and DTR distribution is investigated by performing a K–S test at multiple significance levels ($\alpha$). Depending on $\alpha$, the K–S test might yield a rejection of the null hy-
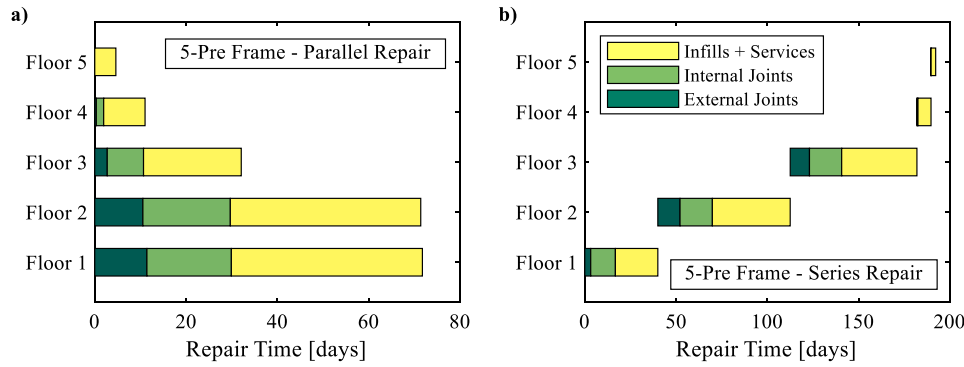
**Fig. 14.** A repair-time realisation at a 712-year $T_r$ for the 5-Pre frame using: a) parallel; and b) in-series repair.
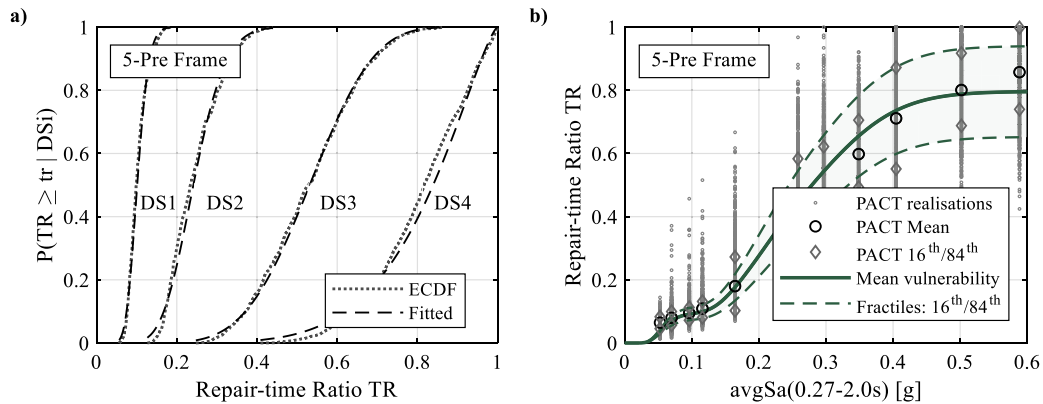


**Fig. 15.** a) ECDFs and beta distributions of the DTRs for the 5-Pre frame; and b) vulnerability function evaluated using the derived DTRs in comparison with loss realisations produced by PACT for the 5-Pre frame.

**Table 7**

Mean $\mu_{DTRi}$ and coefficient of variation $CoV_{DTRi}$ values for the DTRs of all case-study structures.

| DS/Frame | DS1 | | DS2 | | DS3 | | DS4 | |
|---|---|---|---|---|---|---|---|---|
| | $\mu_{DTR1}$ [%] | $CoV_{DTR1}$ | $\mu_{DTR2}$ [%] | $CoV_{DTR2}$ | $\mu_{DTR3}$ [%] | $CoV_{DTR3}$ | $\mu_{DTR4}$ [%] | $CoV_{DTR4}$ |
| 3-Pre | 9.8 | 0.309 | 24.6 | 0.253 | 52.3 | 0.220 | 80.2 | 0.175 |
| 3-Low | 9.9 | 0.248 | 25.1 | 0.322 | 56.2 | 0.182 | 85.2 | 0.139 |
| 3-High | 10.9 | 0.303 | 26.2 | 0.291 | 62.1 | 0.164 | 87.3 | 0.102 |
| 5-Pre | 9.2 | 0.242 | 23.1 | 0.217 | 49.6 | 0.204 | 79.6 | 0.181 |
| 5-Low | 9.5 | 0.303 | 24.3 | 0.289 | 53.0 | 0.201 | 82.9 | 0.151 |
| 5-High | 9.9 | 0.268 | 25.6 | 0.314 | 58.8 | 0.149 | 84.3 | 0.135 |
| 8-Pre | 9.0 | 0.241 | 26.1 | 0.298 | 47.1 | 0.193 | 72.4 | 0.194 |
| 8-Low | 9.2 | 0.316 | 26.5 | 0.303 | 51.3 | 0.172 | 75.1 | 0.145 |
| 8-High | 9.5 | 0.308 | 29.2 | 0.276 | 57.1 | 0.146 | 76.5 | 0.138 |

pothesis (H$_0$), implying insufficient evidence to support the statement that the fitted distributions can characterise the empirical data. Table 8 summarises the α values at which the K–S test does not reject H$_0$, starting with α equal to 5%. It is observed that the vast majority of the fitted beta distributions for DLRs and DTRs related to DS2 to DS4 pass the K–S test at a 5% α. A rejection of H$_0$ is solely encountered on a few occasions, so the α value is reduced to 2–3% to allow such cases to pass the test. Other distributions (*e.g.,* Weibull, lognormal, gamma) were also tested and did not perform better than the beta.

Conversely, most of the distributions fitted for DS1 do not pass the K–S test at a 5%-α, indicating the lack of sufficient evidence to support H$_0$. This implies that more loss/repair-time data for DS1 are needed, particularly those produced by low IM levels. These distributions, however, can pass the test by substantially reducing α and, on multiple occasions, changing the distribution type. For instance, various DLRs of DS1 pass the test upon decreasing α to as low as 0.5–1%, along with

using a lognormal (logn) distribution. The same applies to the DTRs of DS1. Despite these limitations, the building-level loss/repair time estimates obtained via the derived DLRs/DTRs are still highly consistent with those acquired from PACT, at least for the mean values (see Section 4.3). Moreover, the beta distribution remains among the best to statistically characterise consequence models (DLRs and DTRs) [85]; and it has been widely adopted in several studies [15,16].

### 4.6. Comparison of the derived DLRs and DTRs with other studies

The derived DLR and DTR distributions are now compared to those found in the literature. Table 9 reports $\mu_{DLRi}$ values from past studies considering various DSs and building typologies. The average difference between the $\mu_{DLRi}$ values derived for the 5-Pre frame (see Table 6) and those proposed by Martins et al. [13] for mid-rise nonductile Portuguese RC frames does not exceed 3%. This is attributed to the similarities in
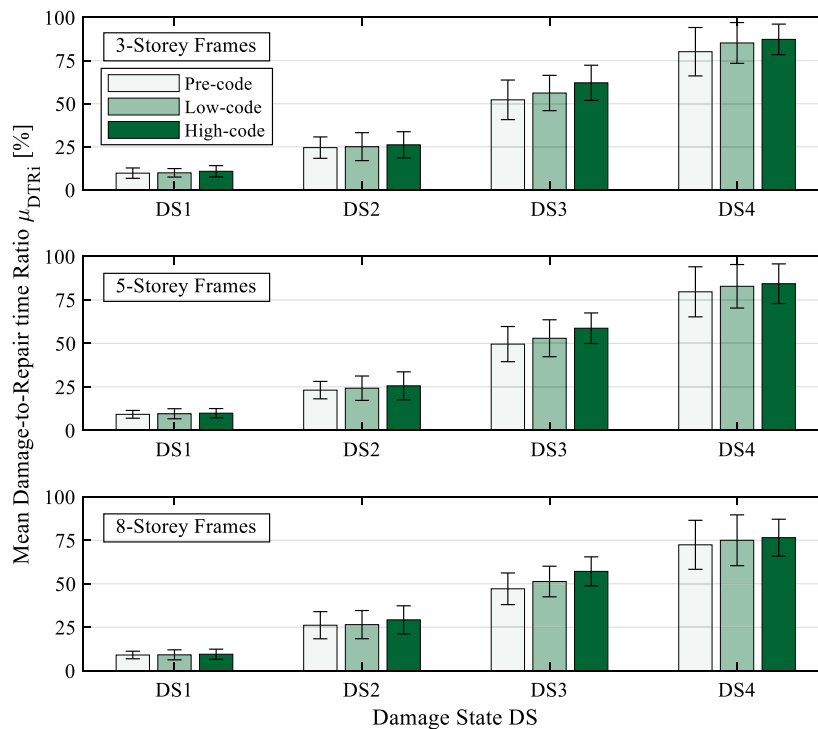
**Fig. 16.** Bar charts for the mean DTR values ($\mu_{DTRi}$) and error bars of $\pm 1\sigma$ for all the case-study frames.

**Table 8**
The minimum α values that allow the fitted DLR and DTR distributions to pass the K–S test.

| DS/ Frame | DS1 | | DS2 | | DS3 | | DS4 | |
|---|---|---|---|---|---|---|---|---|
| | DLR | DTR | DLR | DTR | DLR | DTR | DLR | DTR |
| 3-Pre | 1% | 5% | 5% | 5% | 5% | 2% | 5% | 5% |
| 3-Low | 1%-logn | 1%-logn | 5% | 5% | 1% | 5% | 5% | 1% |
| 3-High | 1%-logn | 5% | 5% | 3% | 5% | 5% | 2% | 5% |
| 5-Pre | 0.5%-logn | 3% | 5% | 5% | 5% | 5% | 5% | 5% |
| 5-Low | 0.5%-logn | 5% | 5% | 2% | 2% | 5% | 5% | 5% |
| 5-High | 1%-logn | 0.5% | 2% | 5% | 5% | 5% | 5% | 5% |
| 8-Pre | 1%-logn | 1%-logn | 5% | 5% | 5% | 5% | 5% | 2% |
| 8-Low | 0.5%-logn | 3% | 5% | 5% | 3% | 5% | 5% | 5% |
| 8-High | 1%-logn | 2% | 2% | 5% | 5% | 5% | 5% | 5% |

design-code level and construction practice. In contrast, remarkable differences of up to 27% are observed when comparing the $\mu_{DLRi}$ values of Martins et al. [13] to the ones derived here for case studies with different heights and code levels, such as the 3-High frame. This signals that the height and design-code level must be carefully considered when selecting DLRs to run building-level loss analysis. The $\mu_{DLRi}$ values in Di Pasquale et al. [14] notably deviate from those derived in this study as the former values are meant for generic Italian buildings (not just RC), and they were derived by expert judgment, making them more suitable for approximate analysis. Similar remarks are drawn about the $\mu_{DLRi}$ values in Dolce et al. [15].

The $\mu_{DLRi}$ values derived by Bal et al. [16] for DS3 and DS4 exceed 100% as they assumed that a structure sustaining such high DSs would be rebuilt rather than repaired. They also accounted for the increased cost due to demolition/debris removal, so it is essential to understand the underlying assumptions before adopting any DLRs to maintain the reliability of loss results. Lastly, it is worth highlighting that the $\mu_{DLRi}$ values derived here differ substantially from those proposed for

multi-family dwellings by HAZUS Technical Manual [6]; a widely used reference for seismic risk modelling in the USA and many other regions. This is attributed to the variation in construction practice between Italy (and the Mediterranean) and the USA. In fact, losses incurred by RC residential buildings in Italy, unlike buildings in the USA, are generally dominated by the damage of infills and their embedded services. Such losses are considerably higher than those incurred by structural components, which explains the relatively larger $\mu_{DLRi}$ values for DS1 to DS3 in this study compared to HAZUS. This means that using HAZUS DLRs for Italian buildings would significantly underestimate seismic risk.

With respect to DTRs, the derived $\mu_{DTRi}$ values are compared to those found in HAZUS for multi-family dwellings. HAZUS specified values equal to 1%, 16.7%, 50%, and 100% for DS1, DS2, DS3, and DS4, respectively. Although the $\mu_{DTRi}$ values for DS3 and DS4 in HAZUS are quite consistent with those derived in this study, the ones related to DS1 and DS2 show a substantial deviation for the same reasons discussed earlier about the difference between Italian residential frames and those commonly built in the USA.

### 4.7. Correlating repair time to direct seismic losses

The DTRs derived in this study are useful for quantifying repair times at a portfolio level and also for computing indirect losses. For residential buildings, indirect losses stem from the cost of relocating occupants to temporary housing facilities due to the downtime caused by ongoing repair works. Therefore, the accurate evaluation of repair time is essential to obtain meaningful indirect-loss estimates. The main issue, however, is the limited availability of DTRs in the literature. A possible workaround is to estimate the repair time (or indirect loss) from direct losses, assuming a nonlinear relationship between both metrics. For instance Calvi et al. [86], proposed a relationship similar in shape to the normal standard CDF, which was also adopted by Gentile and Calvi [87] for loss-based seismic design. This approach sounds rational, but its functional form has not been rigorously calibrated due to the lack of direct-loss vs repair-time data. While calibrating an analytical model for such a purpose is outside the scope of this work, the produced data (realisations) can be utilised to extrapolate qualitative remarks.

**Table 9**
Mean DLR values ($\mu_{DLRi}$) obtained from several studies in the literature.

| Reference | Building description | DS1 | DS2 | DS3 | DS4 |
|---|---|---|---|---|---|
| | | $\mu_{DLR1}$ [%] | $\mu_{DLR2}$ [%] | $\mu_{DLR3}$ [%] | $\mu_{DLR4}$ [%] |
| Martins et al. [13] | Mid-rise older nonductile Portuguese RC frames | 11.7 | 32.1 | 64.5 | 83.5 |
| Dolce et al. [15] | Generic Italian buildings | 3.5 | 14.5 | 30.5 | 80.0 |
| Di Pasquale et al. [14] | Generic Italian buildings | 1.0 | 10.0 | 35.0 | 75.0 |
| HAZUS [6] | Multi-family dwellings | 2.0 | 10.0 | 50.0 | 100.0 |
| Ba et al. [16] | Generic Turkish buildings | 16.0 | 33.0 | 105.0 | 104.0 |



**Fig. 18.** LR vs TR realisations for the 5-Low frame without infills (bare).

For example, Fig. 17a shows the realisations of loss vs repair-time ratios (LR vs TR) obtained from PACT for the 5-Low frame. The colour bar indicates the MIDR value simulated at each realisation. It can be observed that the damage evolution in structural and nonstructural components that occurs when the MIDR values increase, determines the relationship between LR and TR, which can be qualitatively divided into three distinct segments as per the dashed lines. Segment 1 has a linear trend that involves realisations with very low MIDR values (<0.17%), indicating that the damage is limited to infills only, which in turn experience DS1 (or sometimes no damage) as verified by the infill fragility models. Segment 2 can be represented by a downward-concavity curve at which the infills begin experiencing a variety of DSs (i.e., DS1 to DS3), but structural elements are still intact. Finally, segment 3 appears as an upward-concavity curve. It starts at MIDR levels (nearly 0.35% for this case), for which structural elements begin sustaining DS1 or higher. This segment ends at point (1,1). The previous observations are supported by Fig. 17b, which provides the contributions to losses by structural and nonstructural components at the end boundaries of each segment. Further research is needed to fit appropriate analytical models representing the three segments (e.g., polynomial, power law, exponential).

It should be noted that the above remarks are not generic to all building typologies and configurations as there is a strong dependence on the type of structural and nonstructural components and their damage evolution (e.g., acceleration-sensitive components; not modelled in this study). This is exemplified in Fig. 18, where loss analysis is run for the 5-Low frame without taking infills as part of the component inventory. In this case, the LR vs TR relationship can be regarded as a single upward-concavity curve, which differs from that shown in Fig. 17a. Hence, more research is warranted to account for various architectural configurations and understand the effects of nonstructural damage before developing a generalised model that uses direct losses as a proxy for repair time (or indirect losses).
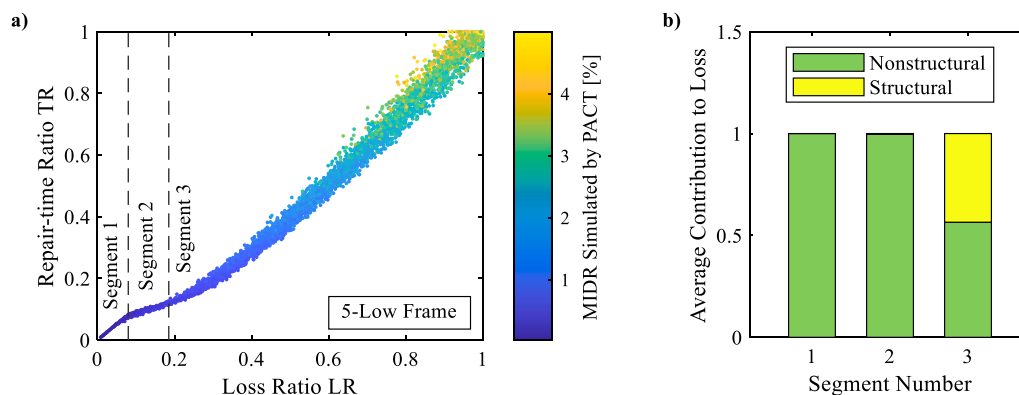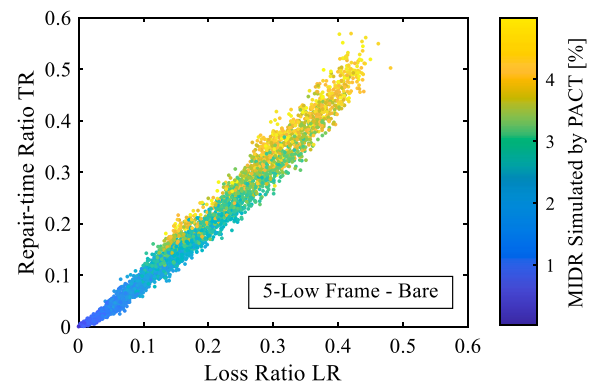
## 5. Concluding remarks

This study demonstrated a simulation-based procedure for deriving the distributions of consequence models that can be used in portfolio risk assessments to provide quick loss estimates at the building's level. This procedure was adopted to derive the distributions of DLRs and DTRs, which are consequence models that quantify direct-loss and repair-time ratios corresponding to multiple structure-specific DSs. Nine case-study RC frames with different heights and design-code levels were specifically developed to reflect common residential RC buildings in Italy (and the Mediterranean). The simulation-based procedure began with defining building-level DSs and their interstorey drift thresholds for each case-study frame. Their dynamic response was then investigated by analysing two-dimensional models via MSA using hazard-consistent record sets. The MSA results were subsequently utilised to generate fragility relationships. Next, FEMA P-58 component-based risk analysis was carried out, adopting a comprehensive inventory of structural and nonstructural components along with their fragility and consequence models, which were developed for Italian structures. The DLRs and DTRs were finally derived by conditioning the resulting loss and repair time realisations on the corresponding global DS for each case-study frame, then fitting a beta distribution to each group of realisations conditioned on the same DS. The derived DLR/DTR distributions were also inspected in terms of goodness-of-fit.

It was observed that the mean DLR and DTR values for the high-code frames are the largest compared to their low-code and pre-code counterparts for the same vertical height. This was attributed to the beam-sway mechanism of the high-code frames that allowed a uniform distribution of deformations along different floors, thus subjecting more components to seismic damage. In contrast, the column-sway behaviour of the pre-code frames led to deformation concentration on a specific



**Fig. 17.** a) LR vs TR realisations for the 5-Low frame; and b) average contribution to loss by structural/nonstructural components near the segment end boundaries.

floor, making the building components on other floors undergo limited damage. It was also noted that the mean DLR and DTR values are the largest for the 3-storey frames, followed by the 5- and 8-storey ones, respectively, for the same design-code level. This could be related to the fact that the first mode becomes less dominant when the height increases, making it challenging to involve all floors in lateral deformation. Lastly, the mean DLR/DTR values were compared to past studies, and significant differences were found as many of such studies considered generic buildings and/or dissimilar assumptions. This signals the importance of adequate selection of DLR and DTR models to assure their compatibility with the structure of interest in terms of typology, construction practice, location, and DS definition.

Finally, the potential of correlating repair time to direct loss was qualitatively explored by studying their variation using the results obtained from PACT. This could be beneficial for estimating the repair time (or indirect loss) from the direct loss in cases where adequate DTRs are unavailable. It was found that the relationship between the two variables could be divided into three different segments (*i.e.*, line, upwards-concavity curve, and downwards-concavity curve). The boundaries between segments depend primarily on the onset of damage in nonstructural and structural building components. However, this outcome is not yet general, and further research is needed to investigate the effect of architectural layouts and nonstructural components different from those implemented in this study.

### Declaration of competing interest

The authors declare that they have no known competing financial interests or personal relationships that could have appeared to influence the work reported in this paper.

### Acknowledgements

### References

[1] De Luca F, Woods GED, Galasso C, D'Ayala D. RC infilled building performance against the evidence of the 2016 EEFIT Central Italy post-earthquake reconnaissance mission: empirical fragilities and comparison with the FAST method. Bull Earthq Eng 2018;16:2943–69. https://doi.org/10.1007/s10518-017-0289-1.

[2] Comerio MC. Estimating downtime in loss modeling. Earthq Spectra 2006;22:349–65. https://doi.org/10.1193/1.2191017.

[3] Sezen H, Moehle JP. Shear strength model for lightly reinforced concrete columns. J Struct Eng 2004;130:1692–703. https://doi.org/10.1061/(ASCE)0733-9445(2004)130:11(1692).

[4] FEMA. Seismic performance assessment of buildings:, vol. 1; 2018 [Methodology. Washington, DC].

[5] Gentile R, Galasso C. Surrogate probabilistic seismic demand modelling of inelastic single-degree-of-freedom systems for efficient earthquake risk applications. Earthq Eng Struct Dynam 2022;51:492–511. https://doi.org/10.1002/eqe.3576.

[6] Fema. Hazus earthquake model technical manual. Fed Emerg Manag Agency 2020:1–436.

[7] Papadopoulos AN, Vamvatsikos D, Kazantzi AK. Development and application of FEMA P-58 compatible story loss functions. Earthq Spectra 2019;55:95–112. https://doi.org/10.1193/102417EQS222M.

[8] Terzic V, Yoo D, Aryan AH. Repair time model for buildings considering the earthquake hazard. In: SEAOC convention proceedings; 2016. p. 562–71.

[9] Cardone D, Flora A, De Luca Picione M, Martoccia A. Estimating direct and indirect losses due to earthquake damage in residential RC buildings. Soil Dynam Earthq Eng 2019;126. https://doi.org/10.1016/j.soildyn.2019.105801.

[10] Martins L, Silva V. Development of a fragility and vulnerability model for global seismic risk analyses. Bull Earthq Eng 2021;19:6719–45. https://doi.org/10.1007/s10518-020-00885-1.

[11] Nafeh AMB, O'Reilly GJ, Monteiro R. Simplified seismic assessment of infilled RC frame structures. Bull Earthq Eng 2020;18:1579–611. https://doi.org/10.1007/s10518-019-00758-2.

[12] Nettis A, Gentile R, Raffaele D, et al. Cloud Capacity Spectrum Method: accounting for record-to-record variability in fragility analysis using nonlinear static procedures. Soil Dynam Earthq Eng 2021;150. https://doi.org/10.1016/j.soildyn.2021.106829.

[13] Martins L, Silva V, Marques M, et al. Development and assessment of damage-to-loss models for moment-frame reinforced concrete buildings. Earthq Eng Struct Dynam 2016;45:797–817. https://doi.org/10.1002/eqe.2687.

[14] Di Pasquale G, Orsini G, Romeo RW. New developments in seismic risk assessment in Italy. Bull Earthq Eng 2005;3:101–28. https://doi.org/10.1007/s10518-005-0202-1.

[15] Dolce M, Kappos A, Masi A, et al. Vulnerability assessment and earthquake damage scenarios of the building stock of Potenza (Southern Italy) using Italian and Greek methodologies. Eng Struct 2006;28:357–71. https://doi.org/10.1016/j.engstruct.2005.08.009.

[16] Bal IE, Crowley H, Pinho R, Gülay FG. Detailed assessment of structural characteristics of Turkish RC building stock for loss assessment models. Soil Dynam Earthq Eng 2008;28:914–32. https://doi.org/10.1016/j.soildyn.2007.10.005.

[17] Del Vecchio C, Eeri M, Di Ludovico M, Prota A. Repair costs of reinforced concrete building components: from actual data analysis to calibrated consequence functions. Earthq Spectra 2020;36:353–77. https://doi.org/10.1177/8755293019878194.

[18] Al-Nammari FM, Lindell MK. Earthquake recovery of historic buildings: exploring cost and time needs. Disasters 2009;33:457–81. https://doi.org/10.1111/j.1467-7717.2008.01083.x.

[19] Mackie KR, Wong J-M, Stojadinovic B. Post-earthquake bridge repair cost and repair time estimation methodology. Earthq Eng Struct Dynam 2010;30:281–301. https://doi.org/10.1002/eqe.942.

[20] Massey FJ. The Kolmogorov-smirnov test for goodness of fit. J Am Stat Assoc 1951;46:68–78. https://doi.org/10.1080/01621459.1951.10500769.

[21] Aljawhari K, Gentile R, Freddi F, Galasso C. Effects of ground-motion sequences on fragility and vulnerability of case-study reinforced concrete frames. Bull Earthq Eng 2020. https://doi.org/10.1007/s10518-020-01006-8.

[22] Aljawhari K, Gentile R, Galasso C. A fragility-oriented approach for seismic retrofit design. Earthq Spectra 2022;38:1813–43. https://doi.org/10.1177/87552930221078324.

[23] Jalayer F, De Risi R, Manfredi G. Bayesian Cloud Analysis: efficient structural fragility assessment using linear regression. Bull Earthq Eng 2015;13:1183–203. https://doi.org/10.1007/s10518-014-9692-z.

[24] Vamvatsikos D, Cornell CA. Incremental dynamic analysis. Earthq Eng Struct Dynam 2002;31:491–514. https://doi.org/10.1002/eqe.141.

[25] Jalayer F, Cornell CA. Alternative non-linear demand estimation methods for probability-based seismic assessments. Earthq Eng Struct Dynam 2009;38:951–72. https://doi.org/10.1002/eqe.876.

[26] Baker JW. Efficient analytical fragility function fitting using dynamic structural analysis. Earthq Spectra 2015;31:579–99. https://doi.org/10.1193/021113EQS025M.

[27] Baker JW, Lee C. An improved algorithm for selecting ground motions to match a conditional spectrum. J Earthq Eng 2018;22:708–23. https://doi.org/10.1080/13632469.2016.1264334.

[28] Kappos AJ, Panagopoulos G, Panagiotopoulos C, Penelis G. A hybrid method for the vulnerability assessment of R/C and URM buildings. Bull Earthq Eng 2006;4:391–413. https://doi.org/10.1007/s10518-006-9023-0.

[29] ISTAT. 15th census of population and housing 2011 (in Italian). 2011.

[30] Del Gaudio C, De Martino G, Di Ludovico M, et al. Empirical fragility curves from damage data on RC buildings after the 2009 L'Aquila earthquake. Bull Earthq Eng 2017;15:1425–50. https://doi.org/10.1007/s10518-016-0026-1.

[31] Rosti A, Del Gaudio C, Rota M, et al. Empirical fragility curves for Italian residential RC buildings. Bull Earthq Eng 2021;19:3165–83. https://doi.org/10.1007/s10518-020-00971-4.

[32] Silva V, Amo-Oduro D, Calderon A, et al. Global earthquake model (GEM) seismic risk map. 2018. 2018.

[33] dei Ministri Consiglio. Regulations for the execution of simple and reinforced concrete constructions. Royal Decree n. 2229 in 16/11/1939. 1939 [In Ital].

[34] Verderame GM, Polese M, Mariniello C, Manfredi G. A simulated design procedure for the assessment of seismic capacity of existing reinforced concrete buildings. Adv Eng Software 2010;41:323–35. https://doi.org/10.1016/j.advengsoft.2009.06.011.

[35] Calvi GM, Magenes G, Pampanin S. Relevance of beam-column joint damage and collapse in rc frame assessment. J Earthq Eng 2002;6:75–100. https://doi.org/10.1080/13632460209350433.

[36] Braga F, De Carlo G, Corrado GF, et al. Meccanismi di risposta di nodi trave-pilastro in ca di strutture non antisismiche. X Congr Naz"L'ingegneria Sismica Ital 2001:9–13.

[37] Masi A, Digrisolo A, Santarsiero G. Concrete strength variability in Italian RC buildings: analysis of a large database of core tests. Appl Mech Mater 2014;597:283–90. https://doi.org/10.4028/www.scientific.net/AMM.597.283.

[38] Verderame Stella A, Cosenza E. Le proprietà meccaniche degli acciai impiegati nelle strutture in c.a. realizzate negli anni '60. X Congr Naz. L'Ingegneria Sismica Ital - ANIDIS; 2001.

[39] Puppio ML, Pellegrino M, Giresini L, Sassu M. Effect of material variability and mechanical eccentricity on the seismic vulnerability assessment of reinforced concrete buildings. Buildings 2017;7:15–7. https://doi.org/10.3390/buildings7030066.

[40] EN 1998-1. Eurocode 8: design of structures for earthquake resistance - Part 1 : general rules, seismic actions and rules for buildings. 2004 [Authority: The

European Union Per Regulation 305/2011, Directive 98/34/EC, Directive 2004/18/EC]. Brussels.

[41] NTC. Norme tecniche per le costruzioni. 2008.

[42] Calvi GM, Bolognini D. Seismic response of reinforced concrete frames infilled with weakly reinforced masonry panels. J Earthq Eng 2001;5:153–85. https://doi.org/10.1080/13632460109350390.

[43] Gentile R, del Vecchio C, Pampanin S, et al. Refinement and validation of the simple lateral mechanism analysis (SLaMA) procedure for RC frames. J Earthq Eng 2021;25:1227–55. https://doi.org/10.1080/13632469.2018.1560377.

[44] Verderame GM, Ricci P, Esposito M, Sansiviero FC. LE CARATTERISTICHE meccaniche degli acciai impiegati nelle strutture in C.A. realizzate dal 1950 al 1980 gerardo mario verderame, paolo ricci, marilena esposito, filippo Carlo sansiviero. 2011.

[45] Sassun K, Sullivan TJ, Morandi P, Cardone D. Characterising the in-plane seismic performance of infill masonry. Bull New Zeal Soc Earthq Eng 2016;49:98–115. https://doi.org/10.5459/bnzsee.49.1.98-115.

[46] De Risi MT, Del Gaudio C, Ricci P, Verderame GM. In-plane behaviour and damage assessment of masonry infills with hollow clay bricks in RC frames. Eng Struct 2018;168:257–75. https://doi.org/10.1016/j.engstruct.2018.04.065.

[47] Del Gaudio C, De Risi MT, Ricci P, Verderame GM. Empirical drift-fragility functions and loss estimation for infills in reinforced concrete frames under seismic loading. Springer Netherlands; 2019.

[48] De Risi MT, Del Gaudio C, Verderame GM. A component-level methodology to evaluate the seismic repair costs of infills and services for Italian RC buildings. Springer Netherlands; 2020.

[49] Liberatore L, Decanini LD. Effect of infills on the seismic response of high-rise RC buildings designed as bare according to Eurocode 8 [Infl uenza della tamponatura sulla risposta sismica di edifi ci in c.a. alti progettati come nudi con l'Eurocodice 8]. Ing Sismica 2011;28:7–23.

[50] Liberatore L, Mollaioli F. Influence of masonry infill modelling on the seismic response of reinforced concrete frames. Civil-Comp Proc 2015:1–17. https://doi.org/10.4203/ccp.108.87.

[51] McKenna F. OpenSees: a framework for earthquake engineering simulation. Comput Sci Eng 2011;13:58–66. https://doi.org/10.1109/MCSE.2011.66.

[52] Priestley MJN, Calvi GM, Kowalsky MJ. Displacement-based seismic design of structures. Pavia: Fondazione EUCENTRE, IUSS Press; 2007.

[53] Karthik MM, Mander JB. Stress-block parameters for unconfined and confined concrete based on a unified stress-strain model. J Struct Eng 2011;137:270–3. https://doi.org/10.1061/(ASCE)ST.1943-541X.0000294.

[54] O'Reilly GJ, Sullivan TJ. Modeling techniques for the seismic assessment of the existing Italian RC frame structures. J Earthq Eng 2019;23:1262–96. https://doi.org/10.1080/13632469.2017.1360224.

[55] Mergos PE, Kappos AJ. A gradual spread inelasticity model for R/C beam-columns, accounting for flexure, shear and anchorage slip. Eng Struct 2012;44:94–106. https://doi.org/10.1016/j.engstruct.2012.05.035.

[56] Zimos DK, Mergos PE, Kappos AJ. Shear hysteresis model for reinforced concrete elements including the post-peak range. In: COMPDYN 2015 - 5th ECCOMAS themat conf comput methods struct dyn earthq eng; 2015. p. 2640–58. https://doi.org/10.7712/120115.3565.1184.

[57] Lavorato D, Fiorentino G, Pelle A, et al. A corrosion model for the interpretation of cyclic behavior of reinforced concrete sections. Struct Concr 2020;21:1732–46. https://doi.org/10.1002/suco.201900232.

[58] Pelle A, Briseghella B, Bergami AV, et al. Time-dependent cyclic behavior of reinforced concrete bridge columns under chlorides-induced corrosion and rebars buckling. Struct Concr 2022;23:81–103. https://doi.org/10.1002/suco.202100257.

[59] Otárola K, Fayaz J, Galasso C. Fragility and vulnerability analysis of deteriorating ordinary bridges using simulated ground-motion sequences. Earthq Eng Struct Dynam 2022;51:3215–40. https://doi.org/10.1002/eqe.3720.

[60] Mohammad Noh N, Liberatore L, Mollaioli F, Tesfamariam S. Modelling of masonry infilled RC frames subjected to cyclic loads: state of the art review and modelling with OpenSees. Eng Struct 2017;150:599–621. https://doi.org/10.1016/j.engstruct.2017.07.002.

[61] Burton H, Deierlein G. Simulation of seismic collapse in nonductile reinforced concrete frame buildings with masonry infills. J Struct Eng 2014;140:1–10. https://doi.org/10.1061/(asce)st.1943-541x.0000921.

[62] Decanini LD, Liberatore L, Mollaioli F. Strength and stiffness reduction factors for infilled frames with openings. Earthq Eng Eng Vib 2014;13:437–54. https://doi.org/10.1007/s11803-014-0254-9.

[63] Silva A, Castro JM, Monteiro R. A rational approach to the conversion of FEMA P-58 seismic repair costs to Europe. Earthq Spectra 2020;36:1607–18. https://doi.org/10.1177/8755293019899964.

[64] Cardone D. Fragility curves and loss functions for RC structural components with smooth rebars. Earthq Struct 2016;10:1181–212. https://doi.org/10.12989/eas.2016.10.5.1181.

[65] Cardone D, Perrone G. Damage and loss assessment of pre-70 RC frame buildings with FEMA P-58. J Earthq Eng 2017;21:23–61. https://doi.org/10.1080/13632469.2016.1149893.

[66] Cardone D, Perrone G. Developing fragility curves and loss functions for masonry infill walls. Earthq Struct 2015;9:257–79. https://doi.org/10.12989/eas.2015.9.1.257.

[67] Romano F, Faggella M, Gigliotti R, et al. Comparative seismic loss analysis of an existing non-ductile RC building based on element fragility functions proposals. Eng Struct 2018;177:707–23. https://doi.org/10.1016/j.engstruct.2018.08.005.

[68] Del Gaudio C, Ricci P, Verderame GM, Manfredi G. Observed and predicted earthquake damage scenarios: the case study of Pettino (L'Aquila) after the 6th April 2009 event. Springer Netherlands; 2016.

[69] Silva A, Macedo L, Monteiro R, Castro JM. Earthquake-induced loss assessment of steel buildings designed to Eurocode 8. Eng Struct 2020;208. https://doi.org/10.1016/j.engstruct.2020.110244.

[70] Kohrangi M, Vamvatsikos D, Bazzurro P. Site dependence and record selection schemes for building fragility and regional loss assessment. Earthq Eng Struct Dynam 2017;46:1625–43. https://doi.org/10.1002/eqe.2873.

[71] Minas S, Galasso C. Accounting for spectral shape in simplified fragility analysis of case-study reinforced concrete frames. Soil Dynam Earthq Eng 2019;119:91–103. https://doi.org/10.1016/j.soildyn.2018.12.025.

[72] Kohrangi M, Bazzurro P, Vamvatsikos D. Vector and scalar IMs in structural response estimation, Part II: building demand assessment. Earthq Spectra 2016;32:1525–43. https://doi.org/10.1193/053115EQS081M.

[73] O'Reilly GJ, Kohrangi M, Bazzurro P, Monteiro R. Intensity measures for the collapse assessment of infilled RC frames. 16th Eur Conf Earthq Eng 2018.

[74] Pagani M, Monelli D, Weatherill G, et al. Openquake engine: an open hazard (and risk) software for the global earthquake model. Seismol Res Lett 2014;85:692–702. https://doi.org/10.1785/0220130087.

[75] Giardini D, Wossner J, Danciu L. Mapping europe's seismic hazard, vol. 95. Washington DC: Eos; 2014.

[76] Baker J, Jayaram N. Correlation of spectral acceleration values from NGA ground motion models. Earthq Spectra - EARTHQ SPECTRA 2008;24. https://doi.org/10.1193/1.2857544.

[77] Akkar S, Bommer JJ. Empirical equations for the prediction of PGA, PGV, and spectral accelerations in europe, the mediterranean region, and the Middle East. Seismol Res Lett 2010;81:195–206. https://doi.org/10.1785/gssrl.81.2.195.

[78] Akkar S, Sandikkaya MA, Ay B. Compatible ground-motion prediction equations for damping scaling factors and vertical-to-horizontal spectral amplitude ratios for the broader Europe region. Bull Earthq Eng 2014;12. https://doi.org/10.1007/s10518-013-9537-1.

[79] Faccioli E, Bianchini A, Villani M. New ground motion prediction equations for T > 1 s and their influence on seismic hazard assessment. In: Proceedings of the university of tokyo symposium on long-period ground motion and urban disaster mitigation; 2010. p. 1–8. March 17-18.

[80] Zhao JX, Zhang J, Asano A, et al. Attenuation relations of strong ground motion in Japan using site classification based on predominant period. Bull Seismol Soc Am 2006;96:898–913. https://doi.org/10.1785/0120050122.

[81] Ozsarac V, Monteiro R, Calvi GM. Probabilistic seismic assessment of reinforced concrete bridges using simulated records. Struct Infrastruct Eng 2021. https://doi.org/10.1080/15732479.2021.1956551.

[82] O'Reilly GJ, Perrone D, Fox M, et al. Seismic assessment and loss estimation of existing school buildings in Italy. Eng Struct 2018;168:142–62. https://doi.org/10.1016/j.engstruct.2018.04.056.

[83] Almufti I, Willford M. Resilience-based earthquake design initiative (REDi™) rating system. 2013.

[84] Molina Hutt C, Vahanvaty T, Kourehpaz P. An analytical framework to assess earthquake-induced downtime and model recovery of buildings. Earthq Spectra 2022. https://doi.org/10.1177/87552930211060856.

[85] Silva V, Crowley H, Varum H, et al. Investigation of the characteristics of Portuguese regular moment-frame RC buildings and development of a vulnerability model. Bull Earthq Eng 2015;13:1455–90. https://doi.org/10.1007/s10518-014-9669-y.

[86] Calvi GM, O'Reilly GJ, Andreotti G. Towards a practical loss-based design approach and procedure. Earthq Eng Struct Dynam 2021;50:3741–53. https://doi.org/10.1002/eqe.3530.

[87] Gentile R, Calvi GM. Direct loss-based seismic design of concrete structures. Earthq Eng Struct Dynam 2022 [under review)].

[88] Ancheta TD, Darragh RB, Stewart JP, et al. NGA-West2 Database. Earthq Spectra 2014;30(3):989–1005. https://doi.org/10.1193/070913EQS197M.